Annikka Weissferdt
Cesar A. Moran

Diagnostic Pathology of Pleuropulmonary Neoplasia

Springer

Diagnostic Pathology of Pleuropulmonary Neoplasia

Annikka Weissferdt • Cesar A. Moran

Diagnostic Pathology of Pleuropulmonary Neoplasia

Springer

Annikka Weissferdt, M.D., FRCPath
Department of Pathology
The University of Texas
MD Anderson Cancer Center
Houston, TX
USA

Cesar A. Moran, M.D.
Department of Pathology
The University of Texas
MD Anderson Cancer Center
Houston, TX
USA

ISBN 978-1-4419-0786-8 ISBN 978-1-4419-0787-5 (eBook)
DOI 10.1007/978-1-4419-0787-5
Springer New York Heidelberg Dordrecht London

Library of Congress Control Number: 2012952999

Printed on acid-free paper

Springer is part of Springer Science+Business Media (www.springer.com)

To my wife, Susan, and my daughters, Kate, Leticia, and Elisa Jean, for their unwavering support and understanding (CAM).
To my family (AW).

Preface

Pleuropulmonary neoplasia is a practical approach to the diagnosis of a diverse group of tumors and pseudotumoral conditions that may appear primarily in the lungs and the pleura. The text of this book has been arranged by family of tumors, which have been divided into types and, in many respects, depending on the cell of origin. In addition, we tried to provide current concepts that are being considered in the evaluation of new nomenclatures and in some cases in the classification of some tumors. Needless to say, in some areas we have taken the liberty of offering our personal opinion based on our experience and that of others from the literature. At the same time, we acknowledge that some of the current concepts may change with time, hopefully leading to further clarification. As we have discussed each entity, we have also provided matching illustrations that the reader of this text may find useful.

In addition, the text provides insights into other areas that are closely related to the diagnosis of pulmonary and pleural tumors, including diagnostic imaging, surgical approach, staging, and molecular diagnostics. For these topics, we are indebted to Dr. Patricia De Groot and Dr. Edith Marom for their chapter on diagnostic imaging, Dr. David Rice for his chapter on surgical approach and staging, and to Dr. Luisa Solis and Dr. Ignacio Wistuba for their chapter on molecular diagnosis. Last but not least, we also want to acknowledge and thank Dr. Francisco Vega for his contribution on the chapter of lymphoproliferative tumors. All these experts have clearly enhanced the usefulness of this text, and we are very grateful for their contributions.

Finally, we hope that the reader will find this book useful in his/her daily practice, not only from the histopathological aspects but also from the radiological, surgical, and molecular aspects of pulmonary and pleural tumors, which in turn should lead to a better understanding of the diverse entities herein discussed.

Houston, TX, USA — Annikka Weissferdt, M.D., FRCPath
Houston, TX, USA — Cesar A. Moran, M.D.

Contents

Contributors

Patricia M. de Groot, M.D. Department of Diagnostic Radiology, The University of Texas MD Anderson Cancer Center, Houston, TX, USA

Edith M. Marom, M.D. Department of Diagnostic Radiology, The University of Texas MD Anderson Cancer Center, Houston, TX, USA

Cesar A. Moran, M.D. Department of Pathology, The University of Texas MD Anderson Cancer Center, Houston, TX, USA

David C. Rice, M.D. Minimally Invasive Surgery Program, Thoracic Surgery, The University of Texas MD Anderson Cancer Center, Houston, TX, USA

Luisa M. Solis, M.D. Department of Pathology, The University of Texas MD Anderson Cancer Center, Houston, TX, USA

Francisco Vega, M.D., Ph.D. Department of Hematopathology, The University of Texas MD Anderson Cancer Center, Houston, TX, USA

Annikka Weissferdt, M.D., FRCPath Department of Pathology, The University of Texas MD Anderson Cancer Center, Houston, TX, USA

Ignacio I. Wistuba, M.D. Department of Pathology and Thoracic/Head and Neck Medical Oncology, The University of Texas MD Anderson Cancer Center, Houston, TX, USA

Diagnostic Imaging of Lung and Pleural Tumors

1

Patricia M. de Groot and Edith M. Marom

Introduction

Diagnosis, staging, and follow-up assessment of thoracic tumors rely heavily on imaging. Communication among clinicians and radiologists is important in optimizing imaging modality selection for these tasks. In this chapter, we present a general overview of imaging of lung and pleural tumors with an emphasis on the strengths and limitations of various imaging methods employed in the evaluation of these malignancies. We emphasize a few pathognomonic imaging findings for which a diagnostic biopsy can be avoided. Our intent is to help guide selection of appropriate imaging, thus decreasing the number of superfluous imaging studies ordered.

Overview of Diagnostic Imaging Methods

Over the past few decades, the use of computers has revolutionized medical imaging, allowing introduction and continual improvement of imaging technologies such as digitized radiography, computed tomography (CT), magnetic resonance imaging (MRI), specialized ultrasound, positron emission tomography (PET), and, most recently, combined PET-CT, which offers simultaneous morphological and physiological imaging. Each of these techniques has benefits and limitations. In some instances, different imaging methods may complement each other in clarifying a particular medical problem. In the diagnosis of tumors, the goal of imaging is to differentiate between benign and malignant tumors to correctly identify patients who need surgery. In addition to determining the resectability of tumors, imaging plays a vital role in selecting the most appropriate surgical approach and identifying tumor recurrence.

Chest Radiography

Chest radiographs effectively demonstrate pulmonary abnormalities because these abnormalities differ in density from the surrounding structures. The density of normal lungs, which contain air, differs significantly from the soft tissue density of tumors, leading to an air-tissue interface at the tumor margins. This interface is responsible for the exquisite display of lung tumors on radiographs. Chest radiography has the benefits of simplicity, low cost, lack of associated pain, and safety, with relatively little radiation exposure to the patient [1]. These benefits make chest radiography the initial imaging modality of choice, in the evaluation of symptoms suspected of originating in the lung or pleura. Although overlapping structures such as bones and crossing pulmonary vessels may mimic pulmonary nodules, the advent of digital radiography and dual energy acquisition has resulted in post-processing techniques that can be used to subtract overlying bones from the lungs and soft tissues and reduce the interference caused by overlapping structures to improve detection of pulmonary parenchymal abnormalities.

After the intraparenchymal location of a pulmonary nodule is established, the next goal of chest radiography is to determine whether it is benign or malignant. In the 1940s and 1950s, researchers attempted to identify radiographic features of benign and malignant disease. Before cross-sectional imaging emerged in the 1980s, definitive preoperative diagnosis of a solitary asymptomatic pulmonary nodule was uncommon; early exploratory thoracotomy was recommended when such indeterminate pulmonary nodules were detected [2, 3]. Although large nodules are more likely than small ones to be malignant, no size criteria allow exclusion of malignancy [4]. Two methods of distinguishing benign and malignant nodules are in use today: (1) documentation

P.M. de Groot • E.M. Marom (✉)
Department of Diagnostic Radiology,
The University of Texas MD Anderson Cancer Center,
1515 Holcombe Blvd., Unit 1478, Houston, TX 77030, USA
e-mail: pdegroot@mdanderson.org; emarom@mdanderson.org

A. Weissferdt, C.A. Moran, *Diagnostic Pathology of Pleuropulmonary Neoplasia*,
DOI 10.1007/978-1-4419-0787-5_1,

of the stability of the nodule over 2 years and (2) identification of benign-appearing calcifications. However, neither method is completely infallible. Specifically, nodule stability has robustly and scientifically proven to be unreliable, as data from the 1950s suggested that it has a positive predictive value of 65 % for benignity [5]. Also, identification of benign calcifications on radiographs has proven to be subjective [6]. However, review of prior radiographs is the most cost-efficient way to assess a pulmonary abnormality. If previous studies are not available for comparison to a current study, then shallow oblique radiographs, fluoroscopy, and/or chest CT scans are the possible next steps in investigation in determining whether a lung or pleural nodule is malignant.

CT

With its better contrast resolution, elimination of overlapping structures, and ability to obtain thin slices, CT is more sensitive than chest radiography in detecting pulmonary nodules (Fig. 1.1a, b) [7] and superior to it in determining the margins and internal characteristics of these nodules. Its disadvantages in comparison with chest radiography are a much higher cost and greater radiation exposure to the patient.

When investigating a pulmonary nodule, in the absence of prior chest radiographs that may have confirmed benignity, a patient is referred for a chest CT scan that will determine the nodule's contours and internal characteristics. Tumor margins may be spiculated, smooth and well circumscribed, or have lobulations (Fig. 1.2a–c). Spiculated margins are highly suggestive of, but not pathognomonic for, malignancy. Spiculations can reflect the presence of peritumoral fibrosis, infiltration of tumor cells into adjacent lung parenchyma, or localized lymphangitic spread [8, 9]. In a study evaluating 634 pulmonary nodules, 50 of 53 nodules (94 %) with diffuse spiculation and 134 of 165 nodules (81 %) with focal spiculation were primary lung carcinomas [10]. Conversely, 8 of 66 (12 %) smoothly marginated, nonlobulated nodules were primary lung tumors, 6 (9 %) were solitary metastases, and 52 (79 %) were benign. Lobulation of margins implies uneven growth that is often associated with malignancy [4], but it is not useful in distinguishing benign and malignant nodules. Also in the study described previously, of 350 smoothly lobulated nodules, 91 (26 %) were primary lung cancer, 57 (16 %) were metastases, and 202 (58 %) were benign [10].

Internal characteristics of pulmonary nodules may include the presence of calcification, macroscopic fat, or hypervascularity, causing intense enhancement on CT scans following administration of intravenous contrast material. Calcification is readily seen on CT scans as very high-density foci measuring more than 200 Hounsfield units (HU). Characteristics of benign calcification include central, diffuse, solid lamination, and a popcorn-like appearance (Fig. 1.3a–d). Solid, central, and laminated calcification typically results from a remote granulomatous infection, whereas popcorn-like calcification is seen with hamartomas. For a nodule to be considered benign, it should display one of these four patterns of calcification and must not have any other features suggestive of malignancy. If calcifications are eccentric, the nodule margins are bilobed, irregular, or spiculated; if the nodule abuts a central bronchus, the nodule should not be considered benign despite the presence of benign-appearing calcification, as calcification can be engulfed by a malignancy [10]. Also, pulmonary metastases

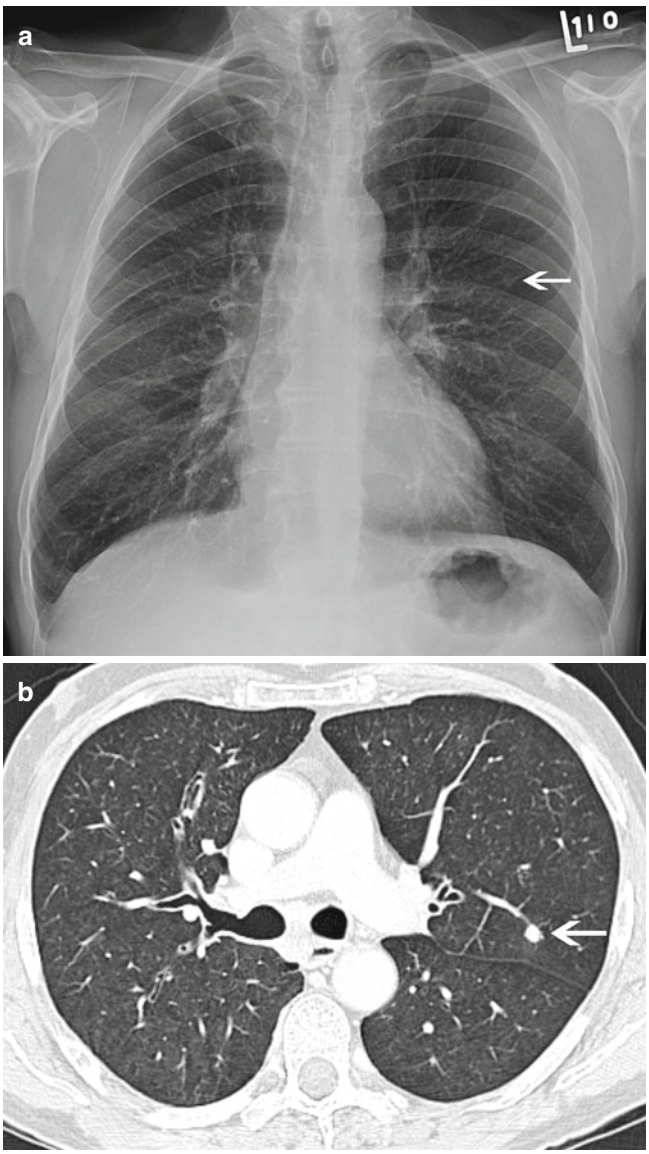

Fig. 1.1 (**a**) Routine chest radiograph showing a small nodule in the right upper lobe that is barely visible (*arrow*) in a 59-year-old man who underwent follow-up assessment after treatment of squamous cell carcinoma of the piriform sinus. (**b**) Contrast-enhanced chest CT scan with lung window settings more readily showing this small 0.6-cm nodule

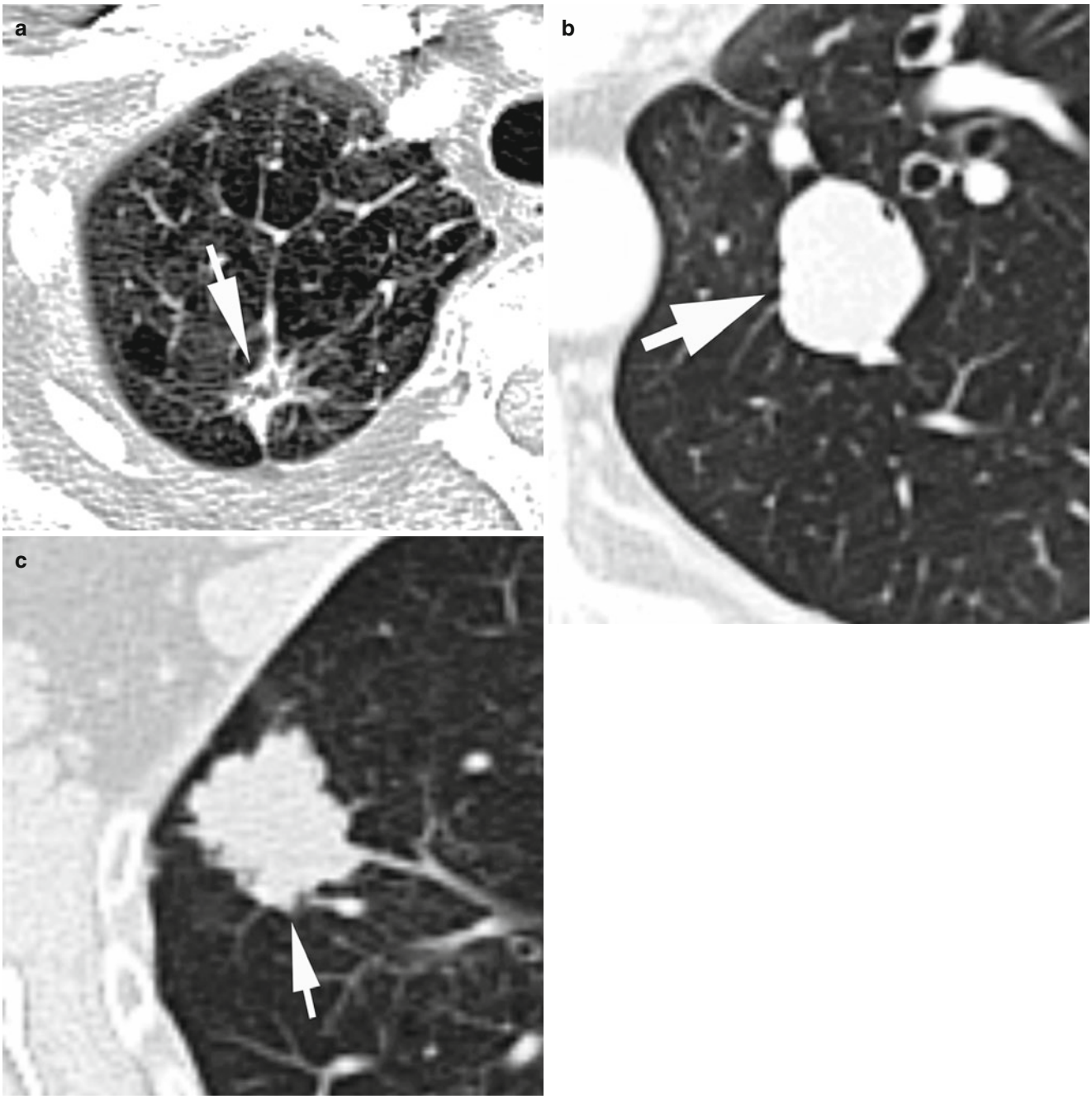

Fig. 1.2 A chest CT scan with lung window settings showing examples of pulmonary tumor margins. Tumor margins may be (**a**) spiculated as in this adenocarcinoma (*arrow*), (**b**) well circumscribed and smooth as in this carcinoid tumor with spindle cell features (*arrow*), or (**c**) lobulated as in this adenocarcinoma with mucinous features (*arrow*)

from osteosarcomas or chondrosarcomas can manifest as nodules with central or solid calcification. Therefore, nodules in patients with one of these cancers cannot be characterized as benign or malignant according to the calcification pattern (Fig. 1.4). In these patients, benignity is established by long-term nodule stability. Another type of calcification, the sand-like, amorphous form, has occurred with 6 % of lung cancers imaged using CT [11] but can also occur with benign disease. This pattern of calcification is not useful for diagnostic purposes.

Most pulmonary nodules imaged using CT are not obviously calcified. Because CT scans can objectively measure nodule density in Hounsfield units, researchers attempted to identify microscopic calcifications in such lesions not obvious to the human eye by measuring their radiodensity in Hounsfield units and establishing a threshold above which

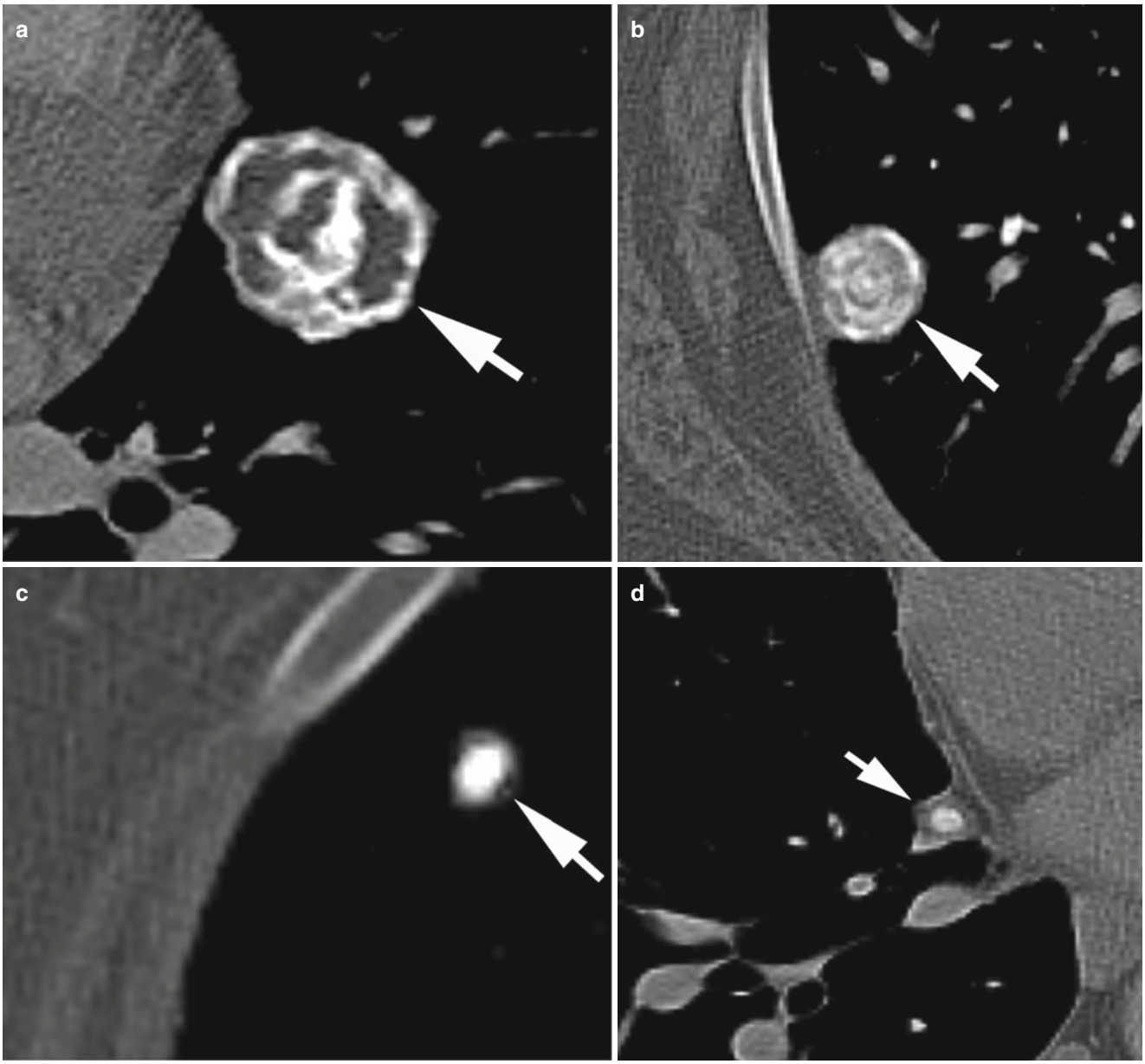

Fig. 1.3 A chest CT scan with bone window settings showing benign patterns of pulmonary nodule calcification (*arrow*). (**a**) Popcorn calcification of a hamartoma in a 27-year-old woman with Carney triad. (**b**) Pulmonary nodule with laminated calcification in a 50-year-old woman with prior histoplasmosis. (**c**) Diffuse solid calcification in a 73-year-old man with a history of histoplasmosis infection. (**d**) Central calcification in a small pulmonary nodule in a 67-year-old man with prior tuberculosis

nodules were to be considered calcified and thus benign, reducing the number of futile thoracotomies [12, 13]. However, more than 10 % of nodules with densities higher than the threshold of 185 HU (above which nodules were posited to be benign) were malignant, and the investigators abandoned the threshold method [13].

Macroscopic fat is also readily recognized on CT scans. A well-demarcated pulmonary nodule containing fat with a density of -40 to -120 HU is considered pathognomonic for a benign hamartoma (Fig. 1.5). Approximately 60 % of hamartomas on thin-section (1 mm) CT scans contain identifiable fat alone or in combination with calcification [14]. Such nodules, even if they grow slowly (doubling time >2 years), are considered benign hamartomas. However, a third of hamartomas do not exhibit calcification or fat on CT scans and thus remain indeterminate nodules.

Air bronchograms are rare in benign pulmonary nodules (6 %) but are readily identified using CT (Fig. 1.6). Their presence is almost always associated with lung cancer of any cell type but is seen most often with adenocarcinoma—both adenocarcinoma in situ (AIS) and more invasive forms [15]. CT can also differentiate among solid nodules, ground-glass

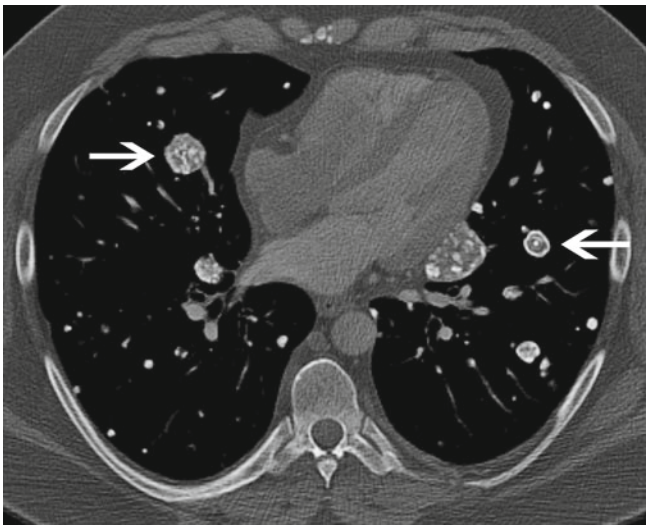

Fig.1.4 Contrast-enhanced chest CT scan with bone window settings showing multiple bilateral calcified pulmonary metastases (*arrows*) in a 38-year-old man with a mesenchymal chondrosarcoma of the left thigh (not shown)

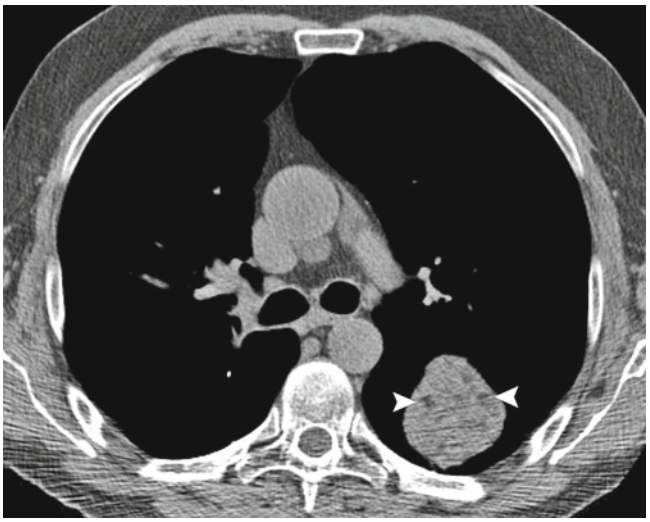

Fig. 1.5 Unenhanced chest CT scan with mediastinal windows showing a 6.5-cm mass in the superior segment of the left lower lobe in a 65-year-old man with treated right upper lobe adenocarcinoma and pulmonary hamartomas. Several foci of very low density in the mass (*arrowheads*) are consistent with macroscopic fat; they are similar to the density of subcutaneous fat and measured -122 HU, making this lesion consistent with a hamartoma. Over a 10-year observation period, this mass had a doubling time of 4 years, compatible with a benign etiology. A similar lesion was resected from the patient at the time of right upper lobectomy for carcinoma that proved to be a hamartoma

nodules (in which the pulmonary vessels can be seen through the nodule), and mixed nodules, which are combined solid and ground-glass nodules (Fig. 1.7). The malignancy rate is highest for mixed nodules (63 %) and is higher for ground-glass nodules (18 %) than for solid nodules (7 %) [16].

Despite the superior sensitivity of CT over radiography in detecting benign pulmonary nodules by identifying fat

Fig. 1.6 Contrast-enhanced chest CT scan with lung window settings demonstrating a 3.4×3.2-cm lobulated mass in the left upper lobe of a 67-year-old woman with lung adenocarcinoma. Multiple small linear lucencies coursing through the tumor are consistent with air bronchograms (*arrowheads*)

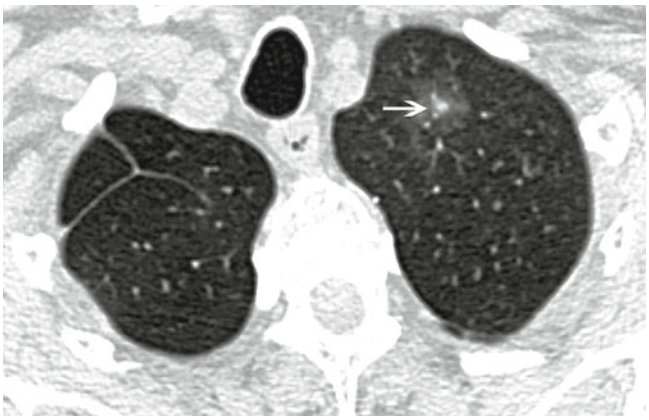

Fig.1.7 Noncontrast thin-section chest CT scan with lung window settings demonstrating a 2.5-cm left upper lobe ground-glass nodule with a central solid component (*arrow*) in a 77-year-old woman 2 years after a right upper lobectomy for an adenocarcinoma in the right upper lobe. Similar nodules were also seen in the remainder of the lobes, which were consistent with multifocal adenocarcinoma of the lung

and calcium, the majority of nodules on initial CT scans remain indeterminate. For further investigation of the indeterminate nodule, studying vascular enhancement may be helpful. The vessels supplying tumors differ both quantitatively and qualitatively from those supplying benign growths and tend to be more "leaky." This inherent difference in blood supply between malignant and benign pulmonary nodules can manifest in differences in their Hounsfield unit values after intravenous contrast agent injection. This method, in which the indeterminate nodule is imaged at intervals before and after intravenous contrast administration, was perfected by Swensen et al. [17, 18]. Absence of significant lung nodule enhancement (≤15 HU) on a CT scan is suggestive of benignity. Although this method is only 77 % accurate and 58 % specific, it does

identify 98 % of malignant nodules and thus can be used to guide follow-up examinations and intervention.

The CT features of pulmonary nodules described herein determine the patients having nodules with benign features not requiring follow-up (benign calcifications or fat), those who would benefit from an immediate biopsy, and those who would benefit from CT-based follow-up to measure nodule growth rates. Determination of a nodule's benignity takes into account patient risk factors such as age and tobacco use, as well as the CT features that are statistically known to be strongly associated with malignancy (e.g., large tumor size, spiculation, mixed solid, and ground-glass appearance). However, radiologists and oncologists should not use the 2-year stability criterion for benignity invariably. This criterion is generally applied to nodules that are solid and larger than 1 cm in diameter. Reliably measuring the growth of nodules smaller than 1 cm can be challenging. Doubling of the volume of a nodule is equivalent to an increase in its diameter of approximately 25 %. Even using CT, visually detecting the doubling of a 4-mm nodule, which is a change in diameter from 4 to 5 mm, is difficult. Thus, small lung tumors can double in volume yet appear to be stable. Even computerized volume measurements are not always accurate with such small nodules, which can appear to change in size with changes in inspiratory effort and slice selection [19]. Ground-glass and mixed solid/ground-glass nodules are most often identified by CT scans, not chest radiographs, and a stability criterion for such nodules on CT scans, such as the 2-year stability rule used for solid nodules on chest radiographs, has yet to be established. In fact, such nodules, which often are detected incidentally or with screening chest CT studies, can have very long doubling times. For example, in a screening study in Japan [20], the mean ± standard deviation doubling times for malignant ground-glass, mixed, and solid nodules were 813 ± 375, 457 ± 260, and 149 ± 125 days, respectively. In fact, 20 % of the nodules in that study had doubling times greater than 2 years; most of those nodules were ground-glass or mixed nodules. Thus, when a ground-glass nodule smaller than 1 cm in diameter is monitored using CT to establish a benign etiology, recent management guidelines suggest a follow-up period of at least 3 years, potentially extending up to 5 years [21].

MRI

The contrast resolution of MRI is superior to that of CT. However, the spatial resolution of MRI is inferior, particularly in the thorax, primarily owing to intrinsic lung characteristics such as low proton density and numerous air-tissue interfaces, as well as examination sensitivity to artifacts from respiratory and cardiac motion. These features make identification of pulmonary nodules smaller than 1 cm difficult. However, once a malignancy is diagnosed, MRI is superior to CT in evaluation of potential soft tissue involvement by the cancer, such as invasion of the chest wall or neural and vascular structures. Small studies showed that dynamic contrast-enhanced MRIs were sensitive in the differentiating of malignant and benign solitary pulmonary nodules that were comparable with the sensitivity of dynamic contrast-enhanced CT, but the nodules investigated using MRI were usually larger than the incidental nodules discovered using CT [22–24].

Because MRI examinations usually take considerable amounts of time, they are often tailored to specific problematic locations, not to searching the entire chest for distant metastatic disease.

PET and Integrated PET-CT

PET with 2-deoxy-D-glucose labeled with ^{18}Fluorine (^{18}FDG) has emerged as a tool for evaluation of suspected and known thoracic malignancies. ^{18}FDG-PET is a physiological imaging technique with poorer spatial resolution than that of anatomic imaging methods such as chest CT and radiography. ^{18}FDG is a glucose analog labeled with a radiotracer, and PET is a technique for assessing glucose use by metabolically active tissues that preferentially take up ^{18}FDG. Many tumors have higher metabolic rates than normal tissue and therefore accumulate ^{18}FDG more intensely than do surrounding tissues. For pulmonary nodules that are indeterminate on CT scans, ^{18}FDG-PET can help identify patients who may benefit from immediate biopsy. Initial studies showed that ^{18}FDG-PET was effective in the differentiation of benign and malignant pulmonary lesions with overall sensitivity, specificity, and accuracy rates estimated to be 96, 88, and 94 %, respectively [25–31]. The combination of ^{18}FDG-PET and CT, known as integrated PET-CT, has provided significantly greater specificity than either CT or PET alone [32].

^{18}FDG-PET does have several limitations. It is neither uniformly specific nor sensitive if the target abnormality is small. In particular, nodules smaller than 1 cm in diameter are not measured accurately and sometimes fall below the resolution of the PET scan [33, 34]. Also, cell type can influence ^{18}FDG uptake. Indolent cancers such as carcinoid tumors, well-differentiated adenocarcinomas, and AIS demonstrate less ^{18}FDG avidity than do other non-small cell lung cancers (NSCLCs) and may exhibit no detectable increase in ^{18}FDG activity above background levels [28, 34–39]. In these instances, the typical morphological features of some of these tumors, such as proximity of a carcinoid tumor to a bronchus or a consolidative tumor, mixed tumor, or ground-glass AIS nodule, should be taken into account when interpreting the results of integrated PET-CT.

In integrated PET-CT studies, quantification of ^{18}FDG uptake using CT for attenuation correction can introduce an artifact related to different breathing states in the nonsimultaneously acquired CT and PET scans, the latter performed without a breath hold. Nodules in the lower lobes of the lungs, which are more affected by respiratory motion than those in the upper lobes, can erroneously exhibit lower ^{18}FDG uptake as a result [40].

Authors have reported false-positive results of studies of primary pulmonary lesions (e.g., a malignancy positive ^{18}FDG-PET result for a lesion that later proves to be benign) in patients with infectious and inflammatory processes such as tuberculosis, histoplasmosis, and rheumatoid nodules [30, 41–46]. The positive predictive value of PET in most patients is high (90 % if the patient is >60 years old) [42, 44]. Lesions with increased ^{18}FDG uptake should be considered malignant until proven otherwise and managed accordingly. A negative PET scan, that is, one in which the nodule does not show increased ^{18}FDG uptake, should serve as a tool for treatment or follow-up planning, not a definitive confirmation of benignity. If biopsy is deferred, a pulmonary abnormality with a negative PET result should be monitored using serial chest CT scans to measure any growth of the lesion. The data reported so far indicate that PET-negative lesions are indolent; thus, this approach using lack of ^{18}FDG uptake to defer immediate biopsy should not adversely affect patient outcome [34].

The use of combined PET-CT studies has enhanced the accuracy of lung cancer staging because these two studies, when integrated, complement each other by overcoming the lack of spatial resolution inherent to PET and lack of physiological information inherent to CT. Therefore, these studies, in combination with clinical and laboratory findings, can be used to determine the necessity of additional imaging studies.

Ultrasound

Ultrasound has a very limited role in the evaluation of patients with intrathoracic malignancies, as the air within the lungs interferes with sound wave transmission. However, it has better soft tissue resolution than does CT and provides real-time imaging throughout the respiratory cycle and therefore can be helpful in limited applications. For instance, regarding imaging of focal chest wall involvement by pulmonary tumors, ultrasound is superior to CT, with a sensitivity rate of 89 % (compared with 40 % for CT), and similarly specific, as both have specificity rates approaching 100 % [47]. Additionally, ultrasound can be used to locate pockets of pleural fluid for diagnostic or therapeutic thoracentesis.

Primary Malignant Lung Tumors

Lung Carcinoma

Despite the advent of new diagnostic techniques, the overall 5-year survival rate for lung cancer, which is the leading cause of cancer deaths, remains about 15 %, and most patients still present with advanced disease [48]. Because lung tumors are encased by the rib cage, early diagnosis of them using physical examination is unlikely. In addition, many lung cancers have no symptoms until they are advanced. In most cases, lung cancer appears as a pulmonary abnormality—a nodule, mass, or consolidation—on chest images. Depending on the stage of the disease, additional smaller nodules, lymphadenopathy, and/or pleural involvement may be present. Over the second half of the twentieth century, multiple studies assessed the efficacy of screening techniques—first chest radiography and later CT—in detection of lung cancer at a stage when cure or control is possible. Nonrandomized uncontrolled screening studies in the 1950s [49–52] gave way to nonrandomized controlled trials [53, 54], which showed that the screened population was more likely than the general population with lung cancer to have their cancer detected at an early stage, to have resectable disease, and to have better survival rates, but without any clear reduction in lung cancer mortality rates. This discrepancy between increased survival rates and stable mortality rates is generally attributed to a combination of lead time, length time, and overdiagnosis bias in screening studies [55].

In the 1970s, four major randomized controlled screening trials, including the Mayo Lung Project, evaluated approximately 37,000 male smokers [56–59], finding that screening chest radiography yielded no change in mortality rates and no reduction in the number of advanced cancers (i.e., no stage shift), although the screened patients had higher 5-year survival rates than the patients who were not screened. A follow-up study more than 20 years after the Mayo Lung Project confirmed the absence of a significant difference in long-term mortality rates for lung cancer [60].

In the late 1990s, advancements in CT technology began to enable detection of pulmonary nodules smaller than 1 cm in diameter in one breath hold and with reduced radiation exposure to the patient using low-dose CT (LDCT). Despite the published 10-year survival rate of 88 % in patients with stage I lung cancer [61] and the increased likelihood that cancers detected using LDCT are operable, screening LDCT in early trials yielded no decreases in the number of advanced lung cancers detected or number of deaths caused by lung cancers compared with historical models in an unscreened population with lung cancer [62].

The largest single randomized lung cancer screening study to date, the National Lung Screening Trial, was launched in 2002 to determine whether screening for lung

cancer using LDCT could reduce mortality rates in patients diagnosed this way with lung cancer. It compared the effect of two screening tests, LDCT and chest radiography, on both lung-cancer-specific mortality and all-cause mortality in persons at high risk for lung cancer, including current and former heavy smokers. From August 2002 to April 2004, the researchers enrolled 53,454 participants, who underwent annual imaging for 3 consecutive years and then underwent follow-up evaluation using questionnaires. Data collection ended on December 31, 2009. This trial demonstrated a relative reduction in the mortality rate for lung cancer with LDCT screening of 20 %. Additionally, the mortality rate for any cause decreased in the LDCT group by 6.7 % [63]. The U.S. Preventive Services Task Force and American College of Radiology are expected to issue recommendations for lung cancer screening in 2012. A current initiative by the United Kingdom Lung Screen is designed to determine whether the results of the National Lung Screening Trial can be replicated in the United Kingdom, with 4,000 patients being randomized to the United Kingdom Lung Screen pilot trial and a goal of 32,000 participants in the main study [64].

Imaging of Lung Cancer Subtypes

Evidence-based guidelines for the management of lung cancer published by the American Society of Clinical Oncology (ASCO) in 2004 [65] recommend initial evaluation of lung cancer using both chest radiography and contrast-enhanced chest CT scanning. The coverage of these CT scans should include the adrenal glands and liver. A ^{18}FDG-PET scan is recommended with the absence of CT evidence of metastatic disease because ^{18}FDG-PET imaging provides improved nodal and distant metastasis staging over CT alone and frequently improves staging to a degree that changes management [66–71]. Imaging does not replace histological sampling of lung masses, but certain subtypes of lung cancer can have typical imaging features.

Primary lung malignancies are grouped into two categories: (1) NSCLC, which accounts for approximately 85 % of all lung cancers and includes several subtypes, such as squamous cell cancer, adenocarcinoma, and carcinoid tumors, and (2) small-cell lung cancer (SCLC).

NSCLC

Squamous cell carcinoma typically originates in the central lung and may cause partial or complete obstruction of a bronchus. Thus, patients with this cancer frequently present with postobstructive pneumonia or atelectasis, which is readily identified on chest radiographs (Fig. 1.8a–d) [72–74]. Less often, patients present with bronchial impaction and distal bronchiectasis associated with air trapping and hyperinflation [73–75]. Approximately one-third of all squamous cell carcinomas originate beyond the segmental bronchi [73, 74]. Because most squamous cell carcinomas grow slowly and become symptomatic because of their central location, extrathoracic metastases are encountered less often in imaging at presentation compared to adenocarcinoma [73]. Also, squamous cell carcinomas are more likely to cavitate than are the other histological subtypes of lung cancer [73]. Cavitation occurs in 10–30 % of squamous cell cancers and is more common in large peripheral masses and poorly differentiated tumors (Fig. 1.9a, b) [73].

Adenocarcinomas typically manifest as peripheral pulmonary nodules or masses. Historically, these nodules typically had soft tissue attenuation and irregular or spiculated margins (Fig. 1.10) [73, 74]. With the expanding use of CT, however, an increasing number of adenocarcinomas present as ground-glass or mixed ground-glass/solid nodules. Investigators have found an association between the spectrum of CT appearances of adenocarcinoma and the classification system proposed by Noguchi and colleagues, in which small (≤2 cm in diameter) peripheral adenocarcinomas are classified into six types based on their growth patterns:

- Type A—localized bronchioloalveolar cell carcinoma (BAC)
- Type B—localized BAC with foci of structural collapse of alveoli
- Type C—localized BAC with active fibroblastic proliferation
- Type D—poorly differentiated adenocarcinoma
- Type E—tubular adenocarcinoma
- Type F—papillary adenocarcinoma with a compressed growth pattern [76–78]

Authors have reported ground-glass attenuation of nodular opacities more often with type A–C than type D–F tumors, whereas they reported soft tissue attenuation more often with type B–F than with type A tumors [76]. The soft tissue attenuation component tends to be absent or account for less than a third of the opacity with type A tumors and account for more than two-thirds of the opacity in type D–F tumors. Mixed nodules with both ground-glass and solid components are more likely to be invasive and at a high stage than are pure ground-glass nodules [79, 80].

Reclassification of lung adenocarcinoma in 2011 by an international multidisciplinary panel consisting of the International Association for the Study of Lung Cancer, American Thoracic Society, and European Respiratory Society introduced new terminology for the different classifications of adenocarcinoma to provide uniformity in the lexicon and diagnostic criteria for this disease [81]. As a result, the terms BAC and mixed-subtype adenocarcinoma are no longer used.

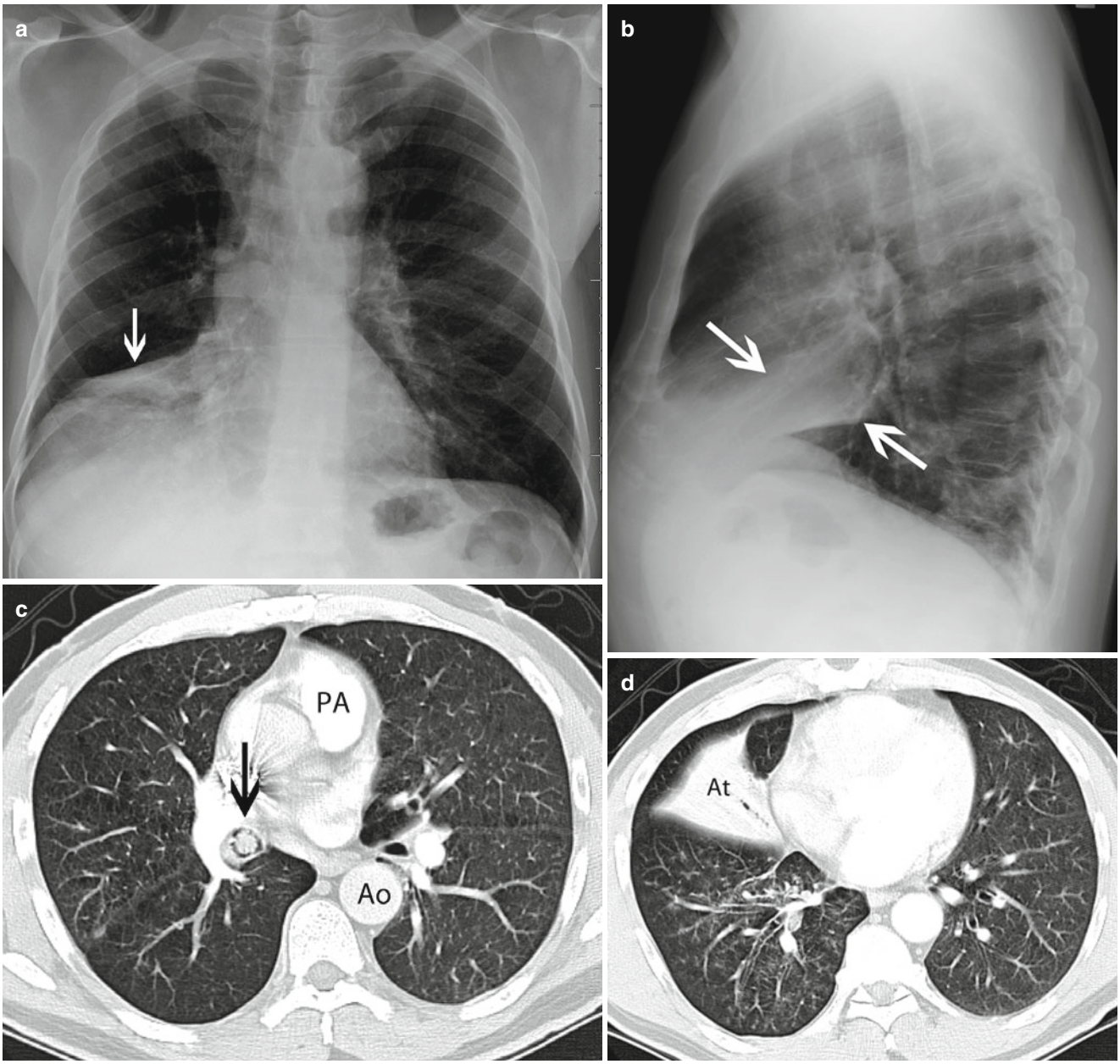

Fig. 1.8 (**a**) Posterior-anterior and (**b**) lateral chest radiographs demonstrating a consolidated collapsed right middle lobe (*arrows*) in a 54-year-old man with endobronchial squamous cell carcinoma of the lung and resultant lobar collapse. (**c, d**) Corresponding contrast-enhanced chest CT scans with lung window settings demonstrating a nodular growth almost filling the lumen of the right bronchus intermedius (*arrow*), resulting in right middle lobe atelectasis (*At*). *PA* pulmonary artery, *Ao* descending aorta

Lung adenocarcinoma is now classified into three main groups. The first group consists of preinvasive lesions and includes atypical adenomatous hyperplasia and AIS (previously BAC) of both the nonmucinous and mucinous type [81]. This group correlates with Noguchi type A and B tumors. Radiologically, the appearance of these tumors ranges from pure ground-glass nodules to ground-glass nodules with internal foci of alveolar collapse.

The second group is minimally invasive adenocarcinoma, a tumor with a predominantly lepidic pattern and invasion of up to 5 mm [81]. These tumors appear as ground-glass nodules with small internal solid foci (i.e., subsolid nodules). Patients with either preinvasive or minimally invasive adenocarcinomas have disease-specific survival rates near 100 % when the tumors are completely resected.

The third group is invasive adenocarcinoma, which includes several histological subtypes according to the predominant cell pattern, including the lepidic, acinar, papillary, micropapillary, and solid patterns [81]. Some invasive adenocarcinomas with lepidic patterns are included in the

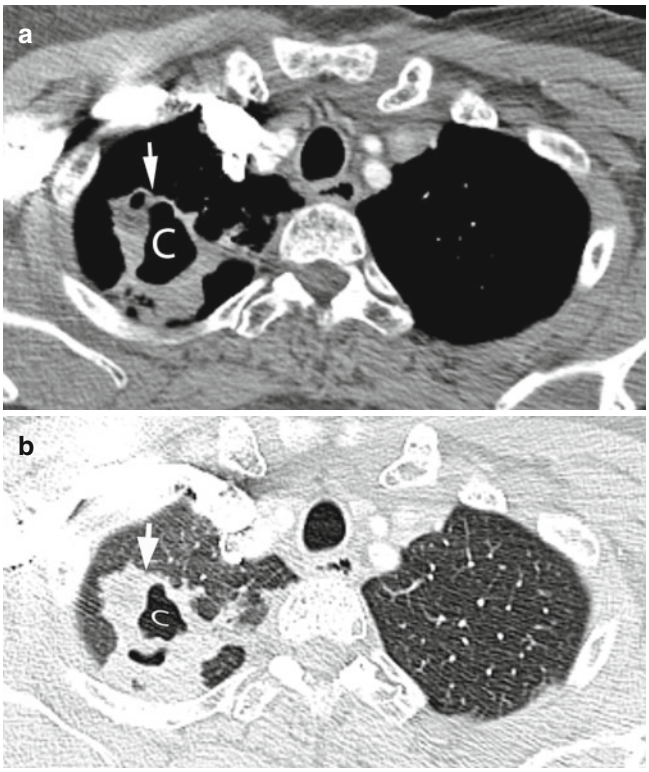

Fig. 1.9 Contrast-enhanced chest CT scan with (**a**) mediastinal window and (**b**) lung window settings showing a 4.0×4.9-cm right apical mass (*arrow*) with central cavitation (*C*) and irregularly thickened walls in a 62-year-old woman with squamous cell carcinoma

Fig. 1.10 Contrast-enhanced chest CT scan with lung window settings demonstrating a 1.9×2.1-cm peripheral nodule in the left upper lobe, with small linear extensions to the adjacent pleural surface and lung (*arrows*), giving it a spiculated appearance, in a 51-year-old woman with primary adenocarcinoma of the lung

Noguchi type C category; the others are included in the Noguchi type D–F categories. The radiological appearances of the invasive adenocarcinomas are usually of a solid nodule with spiculated margins, but distinction between the different subtypes in this invasive group by radiology is not possible.

AIS and minimally invasive adenocarcinomas manifesting as peripheral ground-glass and/or subsolid nodules have appeared as multiple tumors in up to 30 % of reported cases (Fig. 1.11) [76, 82]. These tumors are better seen on chest CT scans and are often not apparent on chest radiographs. Their size may remain stable for many years, with doubling times longer than 2 years. Cystic changes and cavitation occur rarely (≤7 % of cases) [83, 84]. When a nodule of this type exhibits multiple small, focal low-attenuation regions (pseudocavitation) or air bronchograms, the diagnosis of adenocarcinoma should be considered [9, 82, 84, 85]. The mucinous form of AIS infrequently manifests as ill-defined consolidation but should be suspected if the patient's "pneumonia" does not resolve with antibiotic-based treatment. On ^{18}FDG-PET-CT scans, AIS and minimally invasive adenocarcinomas can exhibit low FDG activity, specifically lower than that expected for a malignancy [36, 86, 87].

Large cell carcinoma usually occurs as a peripheral, rapidly growing, poorly marginated mass typically larger than 7 cm in diameter [72–74, 88–90]. Cavitation is uncommon in this tumor.

Carcinoid tumors most often occur as central endobronchial masses with or without associated atelectasis or consolidation; less often, they occur as well-demarcated pulmonary nodules (Fig. 1.12) [91, 92]. These tumors are usually less than 3 cm in diameter, although authors have reported tumors up to 10 cm in diameter [91, 93–95]. Calcification is seen in 25 % of carcinoids on CT scans [92]. Carcinoids can exhibit low ^{18}FDG uptake on PET-CT scans [34, 35, 96], which is attributed to low metabolic activity rates in these often indolent tumors.

SCLC

Primary SCLCs are typically small, centrally located, and associated with marked hilar and mediastinal adenopathy that often engulfs the primary lesion until it is no longer identifiable (Fig. 1.13a, b) [72, 74, 89, 97]. With the increased use of CT and screening CT scans in particular, the number of SCLCs diagnosed as small, early-stage peripheral solitary pulmonary nodules without intrathoracic adenopathy has increased. Historically, as reported in the literature, only 5 % of patients with SCLC have had early-stage disease at presentation [97, 98].

Staging of Lung Cancer

NSCLC

Accurate staging of lung cancer is important to management of and prognosis for this disease. The primary goal of radiological staging is to distinguish potentially resectable (stage I–IIIA) and unresectable (stage IIIB and IV) disease.

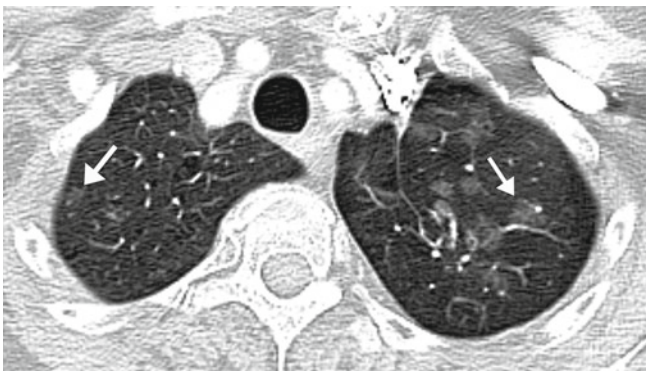

Fig. 1.11 Contrast-enhanced chest CT scan with lung window settings showing multiple ground-glass nodules (*arrows*) compatible with multifocal adenocarcinoma, which was confirmed via biopsy, in a 75-year-old woman 6 years after left upper lobectomy for adenocarcinoma

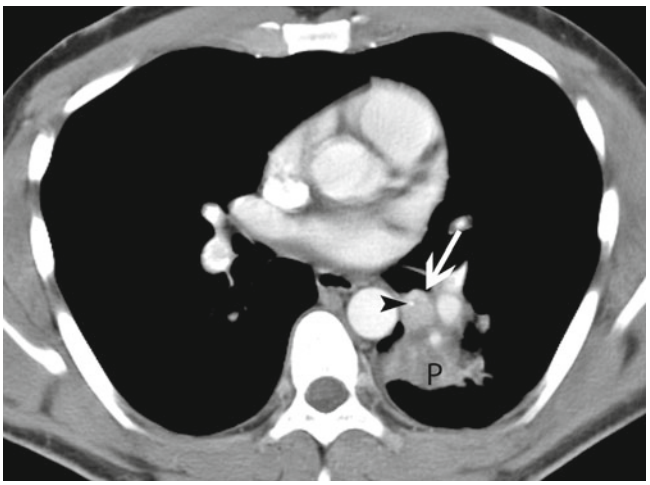

Fig. 1.12 Contrast-enhanced chest CT scan with mediastinal window settings showing a small endobronchial tumor (*arrow*) obstructing the left lower lobe superior segmental bronchus, resulting in postobstructive pneumonia (*P*) of that segment, in a 30-year-old man with a carcinoid tumor. A punctuate calcification is present in the tumor (*arrowhead*)

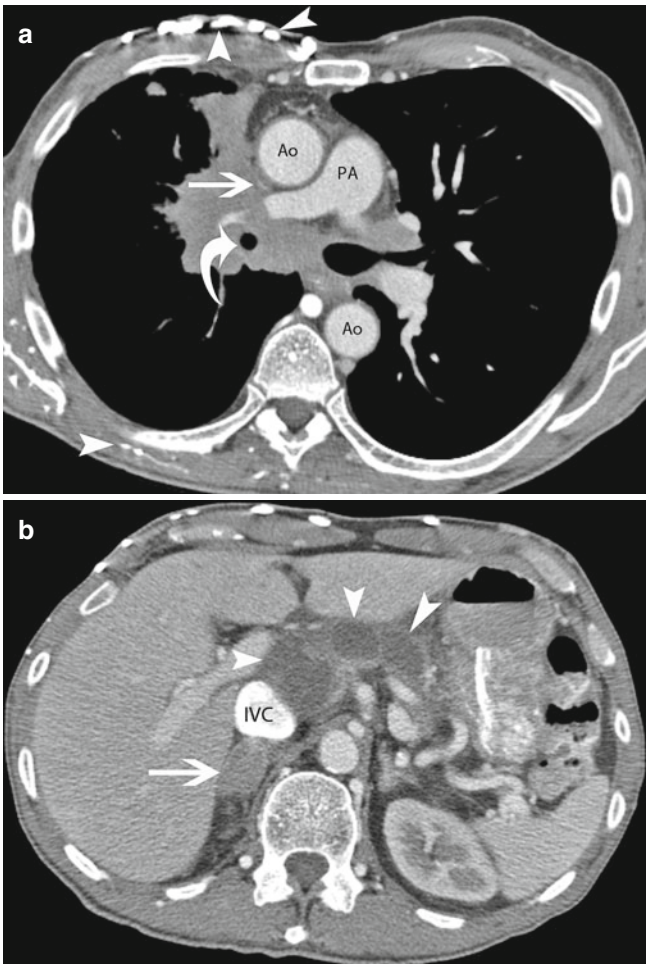

Fig. 1.13 (**a**) Contrast-enhanced chest CT scan with mediastinal window settings showing a confluent right upper lobe tumor and mediastinal and right hilar lymphadenopathy compressing the superior vena cava (*arrow*) in a 66-year-old man with lung SCLC. Numerous dilated collateral vessels in the right anterior chest wall are brightly opacified by the intravenous contrast agent injected from the right arm (*arrowheads*). Also, the bronchus intermedius is markedly narrowed (*curved arrow*) by the tumor encasement. (**b**) CT scan of the upper abdomen in the same patient demonstrating a right adrenal nodule (*arrow*) as well as numerous low-density mesenteric nodal metastases (*arrowheads*), which are compatible with extensive stage SCLC. *Ao* aorta, *PA* pulmonary artery, *IVC* inferior vena cava

Tumor-nodes-metastasis (TNM) staging assesses the primary tumor (T), spread of the tumor into locoregional lymph nodes (N), and distant metastasis of the tumor (M). The original use of TNM staging was with conventional anatomic assessment based on tumor size and morphology, which did not take into account information such as metabolic activity seen on ^{18}FDG-PET scans. However, information from PET scans is now being integrated into TNM staging.

The current staging system for NSCLC is the seventh edition of the TNM system (Tables 1.1 and 1.2) and is based on analysis of long-term survival data on more than 100,000 patients in a study conducted under the auspices of the International Association for the Study of Lung Cancer [99].

Primary Tumor (T Status)

The T status is determined by the size and location of the primary tumor and its degree of invasion into surrounding structures. It is assessed primarily using CT, as the inferior spatial resolution of PET does not lend itself to T staging, which is based on morphological tumor features. However, some evidence indicates that the amount of ^{18}FDG uptake correlates with the prognosis [100–103] and that patients whose primary tumors have high ^{18}FDG avidity, even at an early stage, have shorter survival durations.

Table 1.1 TNM descriptors of NSCLC (International staging system for lung cancer, seventh edition)

T (primary tumor)	
TX	Primary tumor cannot be assessed; tumor proven by the presence of malignant cells in sputum or bronchial washings but not visualized using imaging or bronchoscopy
T0	No evidence of primary tumor
Tis	Carcinoma in situ
T1	Tumor ≤3 cm in greatest dimension surrounded by lung or visceral pleura without bronchoscopic evidence of invasion more proximal than the lobar bronchus (i.e., not in the main bronchus)[a]
T1a	Tumor ≤2 cm in greatest dimension
T1b	Tumor >2 cm but ≤3 cm in greatest dimension
T2	Tumor >3 cm but ≤7 cm in greatest dimension or tumor with any of the following features (T2 tumors with these features are classified as T2a if ≤5 cm) Involves main bronchus, ≥2 cm from the carina Invades visceral pleura Associated with atelectasis or obstructive pneumonitis that extends to the hilar region but does not involve the entire lung
T2a	Tumor >3 cm but ≤5 cm in greatest dimension
T2b	Tumor >5 cm but ≤7 cm in greatest dimension
T3	Tumor >7 cm; tumor that directly invades any of the following: chest wall (including superior sulcus tumors), diaphragm, phrenic nerve, mediastinal pleura, and parietal pericardium; tumor in the main bronchus <2 cm from the carina[a] but without involvement of the carina; tumor-associated atelectasis or obstructive pneumonitis of the entire lung or a separate tumor nodule or nodules in the same lobe
T4	Tumor of any size that invades any of the following: mediastinum, heart, great vessels, trachea, recurrent laryngeal nerve, esophagus, vertebral body, and carina; separate tumor nodule or nodules in a different ipsilateral lobe
N (regional lymph nodes)	
NX	Regional lymph nodes cannot be assessed
N0	No regional lymph node metastasis
N1	Metastasis in ipsilateral peribronchial and/or ipsilateral hilar lymph nodes and intrapulmonary nodes, including involvement via direct extension
N2	Metastasis in an ipsilateral mediastinal and/or subcarinal lymph node or nodes
N3	Metastasis in a contralateral mediastinal, contralateral hilar, ipsilateral or contralateral scalene, or supraclavicular lymph node or nodes
M (distant metastasis)	
MX	Distant metastasis cannot be assessed
M0	No distant metastasis
M1a	Separate tumor nodule or nodules in a contralateral lobe; tumor with pleural nodules or malignant pleural (or pericardial) effusion[b]
M1b	Distant metastasis

Used with permission from Goldstraw et al. [99]

[a]Uncommon superficial spreading tumors of any size with their invasive components limited to the bronchial wall, which may extend proximally to the main bronchus, are also classified as T1 tumors

[b]Most pleural (and pericardial) effusions with lung cancer are caused by the tumor. In a few patients, however, multiple cytopathological examinations of pleural (and/or pericardial) fluid are negative for tumor cells, and the fluid is nonbloody and not an exudate. When these elements and clinical judgment dictate that the effusion is not related to the tumor, the effusion should be excluded as a staging element, and the patient should be classified as having T1, T2, T3, or T4 disease

T status is determined by the tumor size and location and the presence of invasion of adjacent structures in the thorax. The T status descriptors are described in Table 1.1.

Because of its superior spatial resolution over that of MRI and PET, CT more accurately measures the size of primary tumors and readily identifies features of tumors at advanced T stages, such as gross chest wall involvement with rib destruction and bulging chest wall abnormalities. However, CT is not as accurate in identifying more subtle chest wall involvement, such as invasion of the parietal pleura, in contrast with the tumor merely abutting this structure. In one study, CT had a sensitivity rate of 63 % in distinguishing T3–T4 tumors from T0–T2 tumors, and its specificity rate was 84 % [104]. Some CT findings that suggest invasion of the chest wall include obliteration of the extrapleural fat plane, contact of the tumor with the pleural surface more than 3 cm in length, a high ratio of tumor-pleura contact to tumor height, and formation of an obtuse angle between the tumor and the pleura [105]. Despite its superior contrast resolution compared to CT, the accuracy

Table 1.2 NSCLC stage groups and TNM subsets (International staging system for lung cancer, seventh edition

Occult carcinoma	TX	N0	M0
Stage 0	Tis	N0	M0
Stage IA	T1a, b	N0	M0
Stage IB	T2a	N0	M0
Stage IIA	T1a, b	N1	M0
	T2a	N1	M0
	T2b	N0	M0
Stage IIB	T2b	N1	M0
	T3	N0	M0
Stage IIIA	T1, T2	N2	M0
	T3	N1, N2	M0
	T4	N0, N1	M0
Stage IIIB	T4	N2	M0
	Any T	N3	M0
Stage IV	Any T	Any N	M1a, b

Used with permission from Goldstraw et al. [99]

of MRI in identifying chest wall invasion is insufficient and similar to that of CT [104, 106].

For assessment of direct mediastinal involvement of lung tumors, CT and MRI findings suggestive of microscopic invasion of the mediastinum are tumor contact along the mediastinum of more than 3 cm, an angle of contact with the aorta greater than 90°, and a lack of a preserved fat plane between the mass and mediastinal structures [107–109]. Although one study found that MRI was superior to CT in identifying mediastinal invasion by a lung tumor [104], the accuracy of both imaging methods in assessment of mediastinal involvement was disappointing, with sensitivity rates of 55 % for CT and 64 % for MRI [110].

The superb soft tissue contrast resolution and multiplanar capabilities of MRI are ideally suited for evaluation of neurovascular invasion by lung tumors. This is particularly helpful in the evaluation of superior sulcus tumors. An absolute contraindication to surgery for superior sulcus tumors, for which surgical resection in the absence of nodal disease is associated with longer survival durations [111], is invasion of the brachial plexus roots or trunks above the level of the T1 nerve root. Also, the brachial plexus can be readily assessed in the sagittal plane using MRI, but is barely detectable using CT [112]. At the time of imaging, MRI can determine whether the carotid and vertebral arteries are involved by a lung tumor, which is a relative contraindication to surgery. MRI also can determine whether the contralateral vessels are severely affected by atherosclerotic disease, in which case the patient may not be a candidate for surgery [113]. Researchers have developed MRI sequences to overcome flow artifacts and improve vascular and cardiac images in motion. MRI also is used to determine whether and, if so, to what extent a tumor directly involves the heart in the preoperative assessment of surgical candidates.

Nodal Disease (N Status)

The seventh edition of the TNM staging system is identical to the sixth edition in terms of N staging (Table 1.1).

The role of chest radiography in N staging of NSCLC is limited, as mild to modest nodal enlargement is difficult to detect radiographically. Bulky bilateral adenopathy indicates stage IIIB disease. If the patient is too ill or is unwilling to undergo treatment, chest radiography should suffice for staging. In the majority of patients, however, a more accurate staging method is needed.

CT is routinely used for noninvasive N staging of lung tumors. The sole criterion for differentiating benign and metastatic lymph nodes in cross-sectional imaging studies is size: specifically, a short axis diameter greater than 1 cm [114]. Researchers chose this threshold to create a fine balance between sensitivity and specificity in an effort to minimize false-negative results. A meta-analysis that pooled evaluations of the lymph nodes of 5,111 patients with lung cancer in 43 different studies found that the sensitivity and specificity rates for CT in detecting metastases in the mediastinal lymph node compartments according to size criteria were 51 and 86 %, respectively. Similarly, two other meta-analyses showed sensitivity rates of 61–64 % and specificity rates of 74–79 % for CT in distinguishing benign from metastatic lymph nodes [115, 116]. The accuracy of CT in detecting nodal metastases is similar to that of MRI, as the accuracy rates for CT have ranged from 56 to 82 %, whereas those for MRI have ranged from 50 to 82 % [104, 110, 117–120]. These low accuracy numbers result from the fact that normal-sized lymph nodes can harbor tumor cells and, conversely, that nodal enlargement may reflect a benign reactive process [121, 122]. Recent attempts to use MRI to identify lung cancer nodal metastases based on internal characteristics of lymph nodes, such as high signal intensity, eccentric cortical thickening, and obliterated fatty hilum, had similarly disappointing results, with accuracy rates ranging from 70 to 73 % [123, 124].

The accuracy of ^{18}FDG-PET is superior to that of CT in N staging. However, the results of ^{18}FDG-PET performed for this purpose should be interpreted with caution and in conjunction with CT assessment, as nonneoplastic inflammatory processes have increased ^{18}FDG activity. As with that of pulmonary nodules, PET is less accurate than CT in the evaluation of lymph nodes smaller than 10 mm in diameter. N staging using integrated ^{18}FDG-PET-CT is more accurate than that using ^{18}FDG-PET alone [66, 125].

In a pooled analysis of results of multiple studies evaluating a total of 2,865 patients with lung cancer, the sensitivity and specificity rates for ^{18}FDG-PET in identifying metastatic lymph nodes were 74 and 85 %, respectively [126]. In a meta-analysis of 17 studies comprising 833 patients with lung cancer, the overall sensitivity and specificity rates for ^{18}FDG-PET in detecting nodal metastases were 83 and 92 %,

respectively, whereas the sensitivity and specificity rates for chest CT were 59 and 78 %, respectively [127]. In cases with enlarged lymph nodes, the specificity and accuracy of ^{18}FDG-PET and ^{18}FDG-PET-CT decrease, but their sensitivity in detecting nodal metastatic spread increases [128–132]. In one meta-analysis of patients with lung cancer who had enlarged lymph nodes, the median sensitivity and specificity rates for ^{18}FDG-PET were 100 and 78 %, respectively [116]. The lower specificity rate in the presence of enlarged lymph nodes means that almost a quarter of the patients diagnosed with metastatic lymph nodes according to CT and ^{18}FDG-PET findings actually did not have nodal metastasis, but rather had reactive or inflammatory lymphadenopathy. In patients whose mediastinal lymph nodes are smaller than 1 cm in diameter, about 20 % have false-negative PET results; in a meta-analysis of patients with lung cancer, the sensitivity and specificity rates for ^{18}FDG-PET scanning of small nodes were 82 and 93 %, respectively [116].

Because of the accuracies previously described in identifying lymph node metastases, ASCO recommends performing a confirmatory biopsy in lung cancer cases with ^{18}FDG-avid mediastinal lymph nodes so that patients with operable disease will not be denied curative surgery [65]. An ^{18}FDG-PET scan is justified even when a highly suspicious enlarged lymph node is identified on the initial chest CT scan. The ^{18}FDG-PET scan may influence the site of biopsy by identifying a previously unsuspected metastasis (which may upstage the disease), or a metastasis for which biopsy is safer than a biopsy of the initially intended mediastinal lymph node. Whereas mediastinoscopy and transbronchial lymph node biopsy are unable to sample all lymph node stations, tissue sampling remains the most accurate method of preoperative identification of occult metastatic disease in mediastinal lymph nodes smaller than 1 cm in diameter.

Distant Metastasis (M Status)

The goal of identifying of metastatic lung cancer is preventing nontherapeutic thoracotomy. The seventh edition of the TNM staging system divides metastatic disease into M1a for metastases in the thoracic cavity and M1b for extrathoracic metastases. In addition, the M1a category includes malignant pleural effusions and nodules and metastatic pulmonary nodules in the contralateral lung [99]. The common sites of distant metastatic disease in patients with NSCLC are the adrenal glands, liver, brain, and bone.

Establishing the diagnosis of a malignant pleural effusion, an M1a disease [99], is frequently difficult because fluid sampling via thoracentesis is positive for malignancy in only 66 % of patients [133]. Pleural nodules in the presence of pleural fluid are strongly indicative of malignant effusion; however, the pleura does not always exhibit nodularity on CT scans. ^{18}FDG-PET is helpful in identifying pleural metastases, but reported studies of the accuracy of ^{18}FDG-PET in establishing the diagnosis of a malignant effusion are few, with reported sensitivity rates of 92–100 %, specificity rates of 67–71 %, negative predictive values of 100 %, and positive predictive values of 63–79 % [134, 135]. ^{18}FDG-PET scanning for pleural malignancies should be interpreted with caution and in conjunction with CT scanning, as pleural inflammation following talc pleurodesis can persist for years and will exhibit increased ^{18}FDG uptake in the absence of malignant cells [136]. However, a negative PET result, that is, without increased pleural FDG uptake, can be useful in confirming the absence of metastatic pleural disease, particularly when the results of thoracentesis are also negative for metastasis.

In patients with early-stage NSCLC (stage I or II) according to their initial chest CT scans and with no clinical symptoms, additional imaging for metastatic disease has a low yield [137–139]. Some advise further extrathoracic staging of tumors in such patients whose histological type has an increased likelihood of extrathoracic metastasis at the time of presentation, such as adenocarcinoma or large cell carcinoma [19, 137, 140, 141]; however, a study of a large series of patients with early-stage lung cancer did not find this approach to be productive [139]. Nevertheless, a study in which researchers performed biopsy analysis of normal-appearing adrenal glands in patients with NSCLC staged using chest CT found that 12 % of the glands harbored metastatic disease [142]. Another study compared autopsy results with CT scans of the adrenal glands in 73 patients with NSCLC and 18 patients with SCLC within 90 days before death, which showed that CT detected only 20 % of adrenal metastases; the authors attributed this low sensitivity of CT to the absence of substantial structural changes in the glands [143].

Because of these findings, the American College of Chest Physicians [144] and ASCO [65] issued guidelines recommending ^{18}FDG-PET scanning for staging of NSCLC. Further imaging is advised depending on patient symptoms or for abnormal lesions that remain indeterminate following initial investigations using ^{18}FDG-PET and CT. Except in the brain, ^{18}FDG-PET is more sensitive and specific than CT and bone scanning in detecting metastatic disease [145–147]. For example, in a study of 303 patients, the sensitivity and specificity rates for ^{18}FDG-PET in the identification of metastatic disease were 83 and 90 %, respectively [68]. ^{18}FDG-PET also has detected unexpected distant metastases in approximately 15 % of patients with lung cancer [71] and prevented nontherapeutic thoracotomy in 20 % of patients with this disease [68, 69]. PET scanning has the benefits of imaging the entire body in one examination and assessing areas less effectively evaluated using conventional imaging, such as the skin, muscles, and pelvis, facilitating detection of unusual metastatic foci.

The adrenal glands are the most common sites of metastatic disease in patients with NSCLC [148, 149], and isolated

adrenal metastasis occurs in up to 6 % of patients [150]. However, the majority of adrenal nodules, as observed at initial presentation in up to 20 % of patients, are benign [142, 148, 149, 151–159]. Adrenal nodules with a radiodensity of 10 HU or less on CT scans may confidently be diagnosed as adrenal adenomas. This criterion has 98 % sensitivity but only 71 % specificity [160], as 30 % of adenomas do not contain a sufficient amount of lipid to be measured using CT [161]. In these cases, an effective choice is MRI using chemical shift analysis to determine whether microscopic amounts of lipid are present and thus differentiate a benign adenoma from a malignant nodule [162–164]. Chemical shift analyses (MRI) and Hounsfield unit measurements (CT) can be erroneous when the adrenal nodule is small. CT and MRI features of adrenal metastasis include diameter greater than 3 cm, high signal intensity on T2-weighted MRI sequences, poorly defined margins, an irregularly enhancing rim, and invasion of adjacent structures [165].

^{18}FDG-PET can be helpful in establishing the benignity of adrenal nodules. Studies have shown that although the sensitivity and specificity rates for ^{18}FDG-PET scanning of adrenal masses are high (100 and 80–90 %, respectively), adenomas can have increased FDG uptake [146, 166]. The accuracy of identifying an adrenal metastasis is increased when an adrenal nodule has greater ^{18}FDG avidity than the liver as opposed to using a specific standardized uptake value (Fig. 1.14a–c) [167]. Because uptake can be high in adenomas, ASCO recommends biopsy analysis of an isolated adrenal mass identified on imaging studies to rule out distant metastatic disease if the cancer would otherwise be potentially resectable.

NSCLC frequently metastasizes to the liver, but the liver is rarely an isolated site of disease, particularly without evidence of metastatic disease to regional lymph nodes. One meta-analysis found that only 3 % of asymptomatic patients with NSCLC had liver metastases on CT scans. ^{18}FDG-PET can detect liver metastases with accuracy rates ranging from 92 to 100 % [147, 151, 168] and only rare false-positive findings; nevertheless, the data in those studies were limited and were not compared with results of systematic biopsies or state-of-the-art liver imaging with CT or MRI. When a liver lesion is suspected to be a metastasis according to any imaging modality, the suspicion should be confirmed using biopsy if the disease is otherwise potentially resectable [65]. In most cases, liver metastases do not significantly alter management of lung cancer because they are not isolated [169].

Routine screening for brain metastases in asymptomatic patients presenting with newly diagnosed NSCLC remains controversial and is not universally recommended by ASCO [65]. Authors reported that when brain CT was performed in asymptomatic patients undergoing NSCLC staging, the median prevalence of brain metastasis was 3 % (range, 0–21 %) [137, 170–177]. In comparison, when brain CT was performed in a combination of symptomatic and asymptomatic patients, the prevalence of brain metastases was 14 % (range, 6–32 %) [178–186]. Asymptomatic brain metastases are more common in patients with advanced intrathoracic disease than those presenting with early disease [141, 187]. Patients with stage I or II lung cancer have had a brain lesion detection rate of 4 % using CT or MRI, whereas those with stage III disease have had a detection rate of 11.4 % [177]. Although MRI can detect smaller and more numerous brain metastases than CT scan [177], evidence showing that MRI can identify more patients with NSCLC metastases than CT scan is lacking. Consequently, ASCO determined that both CT and MRI are acceptable for evaluation of brain metastases of lung cancer. One of these imaging studies should be performed in patients who have neurological signs of a brain-occupying lesion or have symptoms, as well as asymptomatic patients with stage III lung cancer who are being considered for aggressive local therapy such as thoracotomy or irradiation [65].

^{18}FDG-PET is not recommended for assessment of brain metastases of lung cancer. The sensitivity rate for ^{18}FDG-PET in detection of brain metastases has been shown to be as low as 60 % [147]. ^{18}FDG accumulates avidly in the gray matter, which is the location of most metastatic lesions, thus limiting their detectability.

Although patients with skeletal metastases from lung cancer often are symptomatic and/or have laboratory test results indicating calcium and phosphate level abnormalities [185], one study demonstrated that up to 27 % of asymptomatic patients had skeletal metastases [188]. False-positive abnormalities on technetium 99 m methylene diphosphonate bone scintigrams are numerous, owing to the frequency of degenerative and traumatic skeletal changes which also cause radiotracer accumulation. ^{18}FDG-PET is superior to bone scintigraphy in identifying skeletal metastases. Specifically, ^{18}FDG-PET is able to identify metastatic deposits in the bone marrow that typically are not detected by bone scintigraphy, and ^{18}FDG-PET yields few false-positive results. Furthermore, rates of the specificity, sensitivity, negative predictive value, positive predictive value, and accuracy of ^{18}FDG-PET scanning in the assessment of bone metastases have exceeded 90 % [145, 147, 188, 189]. Bone scintigraphy is therefore considered optional in patients who have evidence of bone metastases according to ^{18}FDG-PET unless they have symptoms suggestive of bone metastases in regions not included on PET scans. Because of the potential for false-positive uptake on both ^{18}FDG-PET scans and bone scintigrams, patients with lung cancer who are candidates for surgery are required to undergo histological confirmation or corroboration of bone metastasis using morphological imaging (radiography, CT, or MRI) of a lesion that will upstage their disease [65].

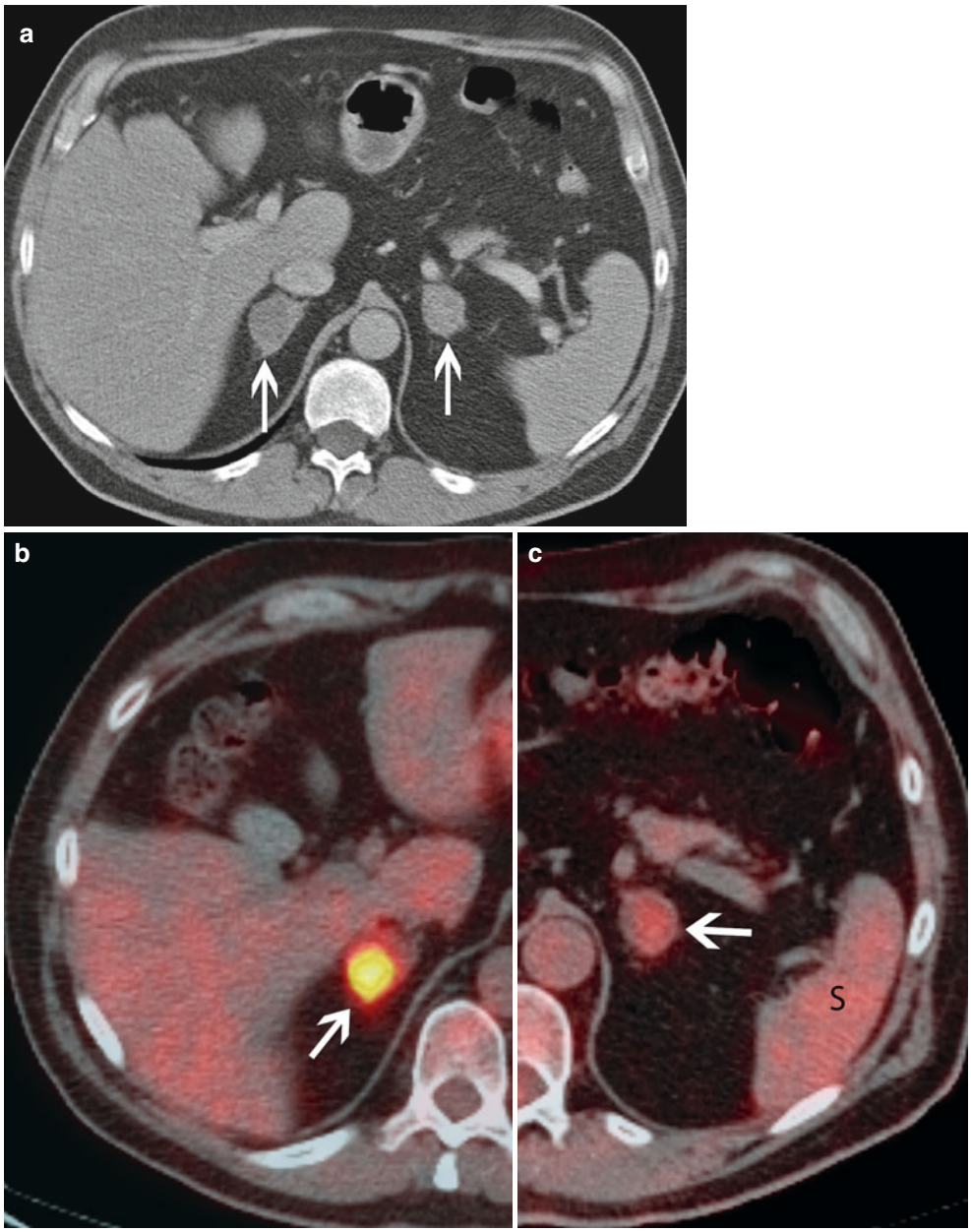

Fig 1.14 (**a**) Contrast-enhanced CT scans with abdominal window settings through the upper abdomen showing bilateral adrenal gland nodules (*arrows*) in a 58-year-old man with metastatic lung adenocarcinoma. (**b**) Fused image from subsequent PET-CT examination showing avid ^{18}FDG uptake in a right adrenal nodule (*arrow*), which was consistent with metastatic disease. (**c**) Fused image from same PET-CT showing background level activity, similar to splenic activity, in a left adrenal nodule, suggesting a benign etiology such as incidental adrenal adenoma. *S* spleen

To summarize staging of NSCLC, imaging with a chest CT scan that includes the adrenal glands and liver is routine. If the disease does not appear to be metastatic, further staging with ^{18}FDG-PET or PET-CT is recommended [65]. Additional imaging, such as brain imaging for early-stage disease or dedicated bone imaging (plain film, scintigraphy, or MRI), is performed if the patient is symptomatic or to clarify uncertain initial ^{18}FDG-PET and CT findings. Patients with locally advanced disease scheduled to receive aggressive therapy (surgery or irradiation) should undergo dedicated brain imaging (MRI or contrast-enhanced CT) even if they are asymptomatic. Biopsy analysis of nodes suspected to have metastases (i.e., those larger than 1 cm in diameter or with increased FDG activity) is required for confirmation of the presence of nodal disease. A positive imaging finding that would change the clinical management of lung cancer, such as an isolated distant metastasis in a patient whose disease is otherwise resectable, should be verified by biopsy.

SCLC

The number of studies on the best imaging methods for staging of SCLC is lower than that for NSCLC, which is probably due to the dismal prognosis of these patients. The great majority of SCLC patients undergo nonsurgical treatment. The Veterans Administration Lung Cancer Study Group developed a simplified method of dichotomous staging of

SCLC [190]. According to this method, limited SCLC includes tumors confined to the hemithorax of origin, mediastinum, and/or supraclavicular lymph nodes. Tumor spread beyond these sites constitutes extensive disease. Most patients with SCLC have disseminated disease at initial presentation [191]. The common sites of metastatic disease are the liver, bone, bone marrow, brain, and retroperitoneal lymph nodes, which can be identified on the initial staging chest CT scan.

Multiple studies, including bone marrow aspiration, brain MRI, CT scanning of the chest and abdomen, and bone scintigraphy, are commonly performed for staging of SCLC [192], but radiologists and oncologists have yet to reach a consensus regarding the routine use of imaging modalities for this purpose. Researchers have attempted to use a single imaging modality for the entire body and reduce the multiplicity of studies currently used for staging of this disease. MRI is able to fill this role, but it has not gained popularity [191]. Staging of SCLC with ^{18}FDG-PET or PET-CT is not recommended according to the second edition of the Evidence-Based Clinical Practice Guidelines of the American College of Chest Physicians [192] because of a lack of randomized prospective trials showing that ^{18}FDG-PET improves staging. Many studies of SCLC have investigated fewer than 50 patients and lacked reference standards to verify the staging accuracy of ^{18}FDG-PET [193–198]. Nevertheless, recent reports suggested that staging of SCLC using ^{18}FDG-PET resulted in a change in management in 8–16 % of patients [199, 200]. As for NSCLC, PET-CT is more accurate than chest CT alone for staging of SCLC but is less accurate than conventional imaging in detecting brain metastases [193–201].

Isolated bone and bone marrow metastases of SCLC are not common [190, 202, 203]. Therefore, evaluation for osseous metastatic disease using bone scintigraphy, bone marrow aspiration, or MRI is not performed in asymptomatic patients with limited SCLC, but rather is usually reserved for patients with extensive disease. Brain metastases, on the other hand, are common in patients with SCLC. Specifically, intracranial lesions are seen at presentation in up to 24 % of asymptomatic patients who undergo contrast-enhanced brain MRI. Therefore, dedicated brain imaging is advocated by many oncologists as part of routine staging workup [191, 204]. Liver and retroperitoneal lymph node metastases are also common at presentation in patients with SCLC but are usually asymptomatic [190, 202]. Thus, staging of SCLC should include contrast-enhanced imaging of the entire liver using either CT or MRI.

Uncommon Primary Pulmonary Malignancies

Some types of primary lung tumors are rare, but when they do occur, they often have radiological features that may suggest their diagnosis.

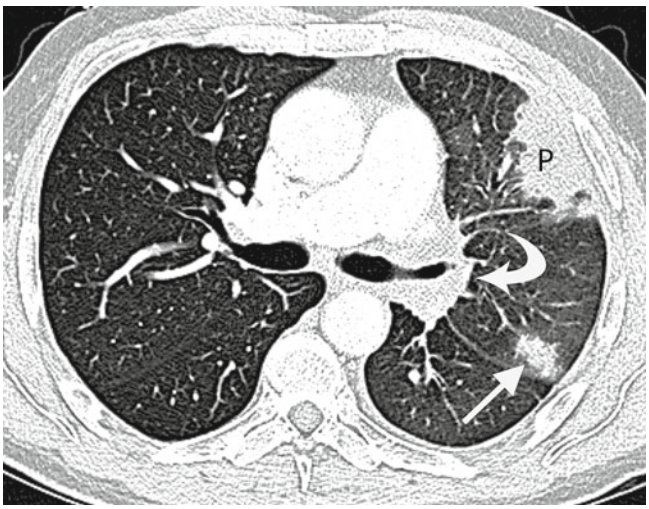

Fig. 1.15 Contrast-enhanced chest CT scan with lung window settings showing a large left upper lobe primary tumor (*P*) and left hilar lymphadenopathy (*curved arrow*) in a 74-year-old man with sarcomatoid carcinoma of the lung. A satellite metastasis (*arrow*) is shown in the same lobe

Sarcomatoid Carcinoma

Carcinomas with pleomorphic, sarcomatoid, or sarcomatous elements are uncommon. On radiological images, these neoplasms can appear either as large peripheral masses or polypoid endobronchial lesions with attendant atelectasis or postobstructive pneumonia [205–208]. Calcification and cavitation are unusual, but necrosis and hemorrhage can appear as heterogeneous attenuation on CT scans [206–208]. Also, hilar and mediastinal adenopathy are uncommon [207]. Pleural effusion can occur as a result of local invasion [209]. Metastases develop in sites similar to those in patients with lung cancer: lung, liver, bones, adrenal glands, and brain (Fig. 1.15) [208].

Pulmonary Blastoma

The typical appearance of pulmonary blastoma is a single, large (2.5–26.0 cm), well-marginated peripheral mass [210–213]. Multiplicity, cavitation, and calcification are rare [213]. Local invasion of the mediastinum and pleura occurs in 8 and 25 % of cases, respectively [211]. Hilar and mediastinal lymph node metastasis occurs in 30 % of resected cases [211]. Extrathoracic metastases are common and have distributions similar to that of primary lung cancer [211, 214].

Neoplasms of the Tracheobronchial Glands

Tracheobronchial gland neoplasms are usually located in the central airways but may occasionally manifest as peripheral pulmonary nodules. These tumors are frequently missed on chest radiographs unless they are large enough to cause obstructions and postobstructive lung parenchymal findings, such as atelectasis or pneumonia, as the tracheal air column

and proximal bronchi are "blind spots" on radiographs for many radiologists. CT, which readily demonstrates the airways, is an important diagnostic tool for adult patients who present with new-onset "asthma."

Adenoid cystic carcinomas are confined to the trachea or main central bronchi in 80 % of patients, whereas 10–15 % of these tumors may manifest as peripheral pulmonary nodules [215–218]. The typical radiological appearance of an adenoid cystic carcinoma is an endotracheal or endobronchial mass, usually lobulated or polypoid, that narrows the airway lumen (Fig. 1.16). These lesions can be circumferential and may manifest as diffuse stenosis [219]. Metastatic spread of an adenoid cystic carcinoma has a distribution similar to that of metastatic spread of NSCLC [218]. Adenoid cystic carcinomas exhibit slow, progressive local growth [216] and metastasize at a late stage; consequently, patients with this cancer are usually considered candidates for surgery. CT is used for surgical planning and readily demonstrates the extratracheal extent of these tumors. However, CT can underestimate the longitudinal extent of an adenoid cystic carcinoma [220] even when it is evaluated in multiplanar reformatted reconstructions, as this tumor has a tendency to infiltrate beneath the mucosa, a microscopic phenomenon that is not identifiable on CT scans.

Mucoepidermoid carcinomas typically occur as central endobronchial masses in the main or lobar bronchi. Less common presentations include a polypoid intraluminal nodule in the trachea and pulmonary nodule or mass in the lung periphery [221–223]. Mucoepidermoid carcinomas are usually slow-growing, low-grade neoplasms with benign clinical courses, although some have more aggressive high-grade features [223–225]. These two forms, adenoid cystic and mucoepidermoid carcinomas, have similar radiological appearances and thus cannot be distinguished from each other using imaging studies alone [223].

Malignant Mesenchymal Lung Tumors

Spindle cell sarcomas (malignant fibrous histiocytoma, hemangiopericytoma, fibrosarcoma, leiomyosarcoma, and synovial sarcoma) are the most common primary pulmonary sarcomas [226–229]. They are most often located in the periphery of the lung, although central and endobronchial masses can occur [227, 228, 230–232]. Authors have reported spindle cell sarcomas as large as 25 cm in diameter; their large size at presentation probably results from their slow growth and tendency to metastasize late. These tumors are typically sharply marginated and occasionally calcified [226–228, 230, 233]. Cavitation is uncommon, although heterogeneous attenuation resulting from necrosis in the mass may be seen on CT scans [226, 233]. In particular, the rich vascularity of hemangiopericytomas in the lung can be demonstrated using CT, MRI, and ultrasound, but this tumor cannot be radiologically distinguished from other sarcomas,

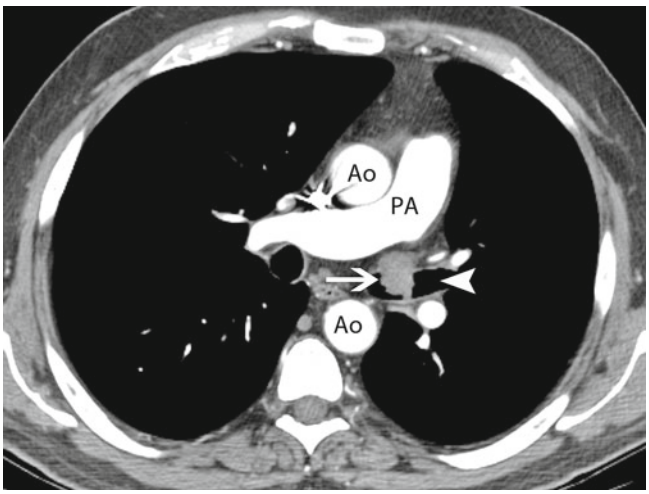

Fig 1.16 Contrast-enhanced chest CT scan with mediastinal window settings showing an irregular nodule (*arrow*) in the left main bronchus with both endobronchial and extrabronchial extension in a 51-year-old man with primary adenoid cystic carcinoma of the left bronchus. Because the tumor did not completely obstruct the airway, the distal left main bronchus (*arrowhead*) remained patent. *Ao* aorta, *PA* pulmonary artery

which can contain similar-appearing vascularity. Features of these tumors that suggest hypervascularity include feeding arteries that can be visualized directly using CT or MR angiography and indirect signs such as avid nodule enhancement on contrast-enhanced chest CT or MRI scans. Evidence of internal hemorrhaging includes high attenuation on unenhanced chest CT scans and hyperintense areas on both T1- and T2-weighted images [232, 234, 235].

Sarcomas of vascular origin (angiosarcomas and epithelioid hemangioendotheliomas) are extremely rare primary lung tumors [228, 236, 237]. Angiosarcomas of the lung are described as multiple bilateral nodules, but most probably represent metastases, and a primary tumor located outside the lung that must be excluded [228]. Pulmonary epithelioid hemangioendothelioma usually appears radiologically as multiple 1–2-cm bilateral pulmonary nodules, although about 25 % of patients have single nodules and unilateral distribution [236, 238, 239]. Authors recently described irregular thickening of the bronchovascular bundles and perilobular structures caused by lymphangitic spread and associated multiple bilateral pulmonary nodules on high-resolution CT scans [240]. Calcification is rarely detected radiologically but is frequently detected histologically [238, 239]. Although primary lung sarcomas are usually indolent, the presence of hemorrhagic pleural effusion is a sign of poor prognosis [236].

Primary Lung Lymphoma

The radiological findings for primary lymphoma of the lung may vary according to the criteria used to define this disease. The most widely accepted definition is intrathoracic

monoclonal lymphoid proliferation without extrathoracic sites of disease at presentation and for at least 3 months after diagnosis. Some authors restrict the diagnosis to pulmonary parenchymal disease only, whereas others include hilar adenopathy with or without mediastinal adenopathy [241–247]. The parenchymal manifestations of lymphoma include solitary or multiple nodules or masses, focal or multifocal consolidation, reticulonodular opacities, and atelectasis (Fig. 1.17) [242, 248–252]. Hilar adenopathy is rare, and pleural effusion occurs in 7–25 % of patients [242, 249, 253].

Secondary Malignant Lung Tumors

Metastasis to the lungs occurs via multiple routes: the pulmonary and bronchial arteries, lymphatics, and airways. The four patterns of metastasis to the lung parenchyma are parenchymal nodules, interstitial thickening (lymphangitic carcinomatosis), tumor emboli with or without pulmonary hypertension or infarction, and airway obstruction by an endobronchial tumor.

Parenchymal nodules are the most common manifestations of metastatic disease in the lungs and are usually multiple and predominantly located in the lower lobes (Fig. 1.18) [254]. When multiple pulmonary nodules are present, they are usually well demarcated, although they may have irregular margins as seen with some adenocarcinomas [255]. They can vary in size from large "cannonball" metastases, as seen with sarcomas, to multiple, small 1-mm nodules distributed in a miliary pattern, as seen with thyroid cancer (Fig. 1.19a, b).

Use of multidetector spiral CT, with improved resolution and decreasing slice thickness, has led to increased sensitivity in the detection of pulmonary nodules. However, the appearance of these nodules on CT is not specific, and many of the nodules identified using CT are benign. When pulmonary nodules are new, growing, and multiple in a patient with a primary malignancy, they are most likely metastases. When an oncologist is in doubt about whether they are metastases, he or she should consider biopsy analysis of the largest nodule. Monitoring of small nodules (<4 mm in diameter) in a patient with a known malignancy is recommended for assessment of their growth, as these nodules are below the resolution of PET.

Solitary lung metastases are uncommon, as researchers have observed them in 2–10 % of patients presenting with pulmonary nodules [2, 10, 256]. Certain primary malignancies are more likely than others to metastasize to the lung in the form of a solitary nodule, including sarcoma, melanoma, and carcinoma of the colon, kidney, testicle, or breast [2, 257, 258]. Reliable radiological criteria distinguishing a primary lung tumor from a solitary pulmonary metastasis are lacking [10, 256] because their imaging features overlap.

Pulmonary metastatic nodules may have an unusual appearance. Cavitation in metastatic nodules is detected using chest radiography in approximately 4 % of patients with metastases, most often those of squamous cell histology (Fig. 1.20a–c) [259, 260]. On CT scans, however, cavitation is seen in 9 % of metastatic nodules, with equal distribution of the adenocarcinoma and squamous cell carcinoma subtypes of NSCLC [261]. Metastatic sarcoma also can cavitate, and a pneumothorax can be the presenting feature of the disease [262, 263]. As described previously, pulmonary

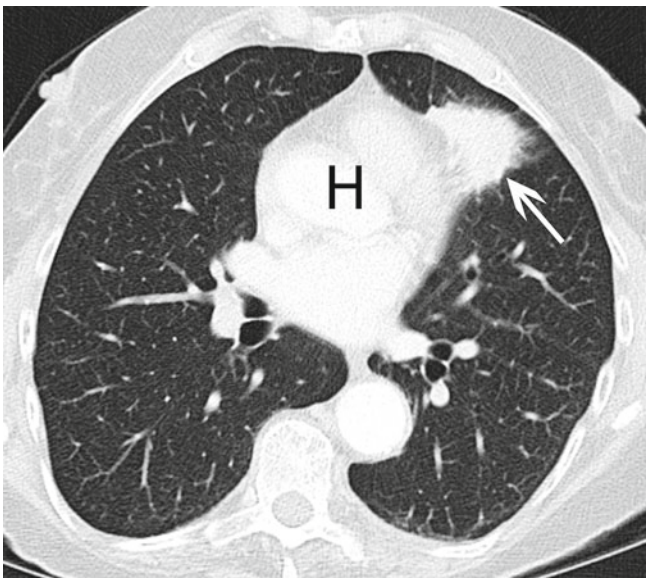

Fig. 1.17 Contrast-enhanced chest CT scan with lung window settings demonstrating an irregular consolidative mass in the lingula (*arrow*) in an 81-year-old woman with primary B-cell lymphoma of the lung. *H* heart

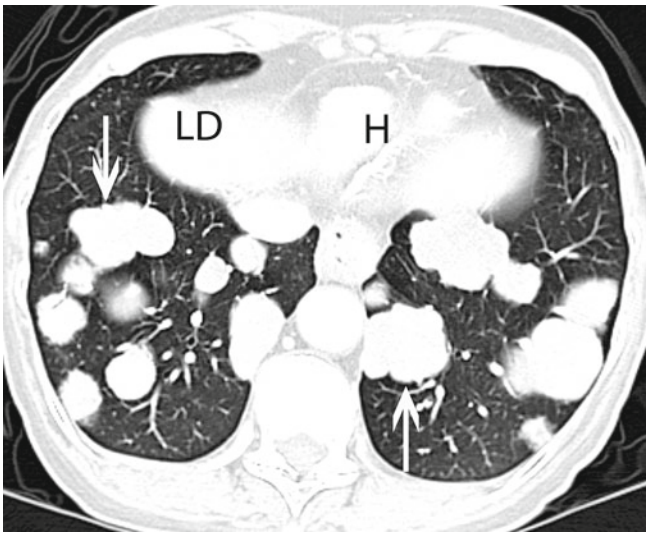

Fig. 1.18 Contrast-enhanced chest CT scan with mediastinal window settings showing a very large number of rounded, well-circumscribed bilateral pulmonary nodules (*two marked with arrows*) with a lower lobe predominance in a 68-year-old woman 3 years after treatment of an adenoid cystic carcinoma in the right neck. Biopsy analysis demonstrated a metastatic adenoid cystic carcinoma, cribriform type. *LD* liver dome, *H* heart

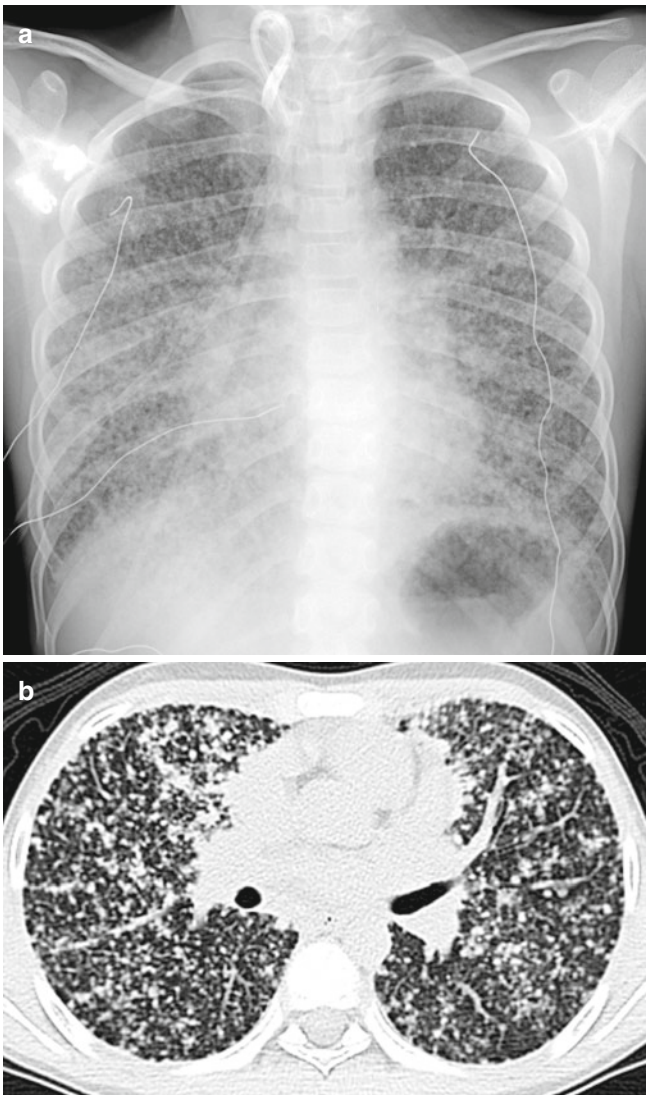

Fig. 1.19 (**a**) Chest radiograph demonstrating a very large number of diffuse bilateral nodules approximately 3 mm in size in diameter in a 13-year-old boy with metastatic papillary thyroid cancer. (**b**) Noncontrast chest CT scan with lung window settings through the mid-lungs confirming the presence of bilateral miliary nodules in a random distribution

nodules with certain calcification patterns are considered benign except in patients with primary osteosarcoma or chondrosarcoma, as calcification and ossification can occur in pulmonary metastases of these tumors [262]. Calcification in pulmonary metastases of other primary malignancies is much less common, but authors have reported it in patients with synovial sarcoma, giant cell tumors of the bone, and carcinomas of the colon, ovary, breast, and thyroid [262, 264–266]. A solid pulmonary nodule surrounded by a ground-glass halo suggests peritumoral hemorrhage (Fig. 1.21) [255] but should be distinguished from other disease processes that have this appearance, such as invasive fungal infections, AIS, and lymphoma [267–269].

Lymphangitic carcinomatosis is uncommon but can occur in patients with primary tumors in the lung, breast, stomach, pancreas, prostate, cervix, or thyroid [262, 270]. Chest radiographic findings of lymphangitic carcinomatosis may mimic those of pulmonary edema, from which it must be distinguished, and include thickened bronchovascular markings, interlobular septal thickening, and, in some cases, pleural effusion [271, 272]. Up to 50 % of patients with pathologically proven lymphangitic carcinomatosis have normal-appearing chest radiographs [273, 274]. A study showed that the use of chest CT, in addition to a chest radiograph, increased the rate of confident diagnosis of lymphangitic carcinomatosis from 54 % (by clinical examination, history, and chest radiography alone) to 92 %, whereas a lack of imaging resulted in no confident diagnoses [275]. On thin-section CT scans, lymphangitic carcinomatosis typically appears with irregular nodular thickening of the interlobular septa and peribronchovascular bundles [272, 276]. This pattern of interstitial thickening causes a CT appearance of polygonal shapes with a central dot superimposed on the normal lung architecture (Fig. 1.22). This appearance, in association with nodularity of the interlobular septa, is pathognomonic for lymphangitic carcinomatosis and distinguishes it from pulmonary edema, in which septal thickening is smooth [277]. When nodularity is not seen, the nondependent distribution and asymmetry of lymphangitic carcinomatosis may help differentiate it from edema. Approximately 30 % of patients with lymphangitic carcinomatosis also present with pleural effusion, and 40 % present with mediastinal or hilar adenopathy [272].

Tumor emboli are rarely identified using imaging despite being observed microscopically in as many as 26 % of patients with lung metastases at autopsy [278, 279]. These emboli are usually located in small or medium-sized pulmonary arteries, which make radiology-based diagnosis of them difficult [280]. On CT scans, tumor emboli appear as dilation or beading of the subsegmental arteries (Fig. 1.23a, b), which may be accompanied by peripheral wedge-shaped areas of low parenchymal attenuation owing to pulmonary infarction [281–283]. Researchers have described the tree-in-bud appearance (branching peripheral centrilobular opacities) as a manifestation of pulmonary tumor embolism [284, 285]. Tumors frequently associated with pulmonary tumor emboli are hepatomas, breast and renal cell carcinomas, gastric and prostatic cancers, and choriocarcinomas [279, 280].

Endobronchial metastasis is uncommon, and its origin is most frequently renal, colorectal, or breast carcinoma or melanoma [286–291]. Secondary chest radiography findings of endobronchial metastases are caused by bronchial obstruction and include atelectasis, postobstructive pneumonitis, and air trapping. On CT scans, endobronchial metastases appear as polypoid, sometimes branching intraluminal soft tissue masses (Fig. 1.24a, b) [292].

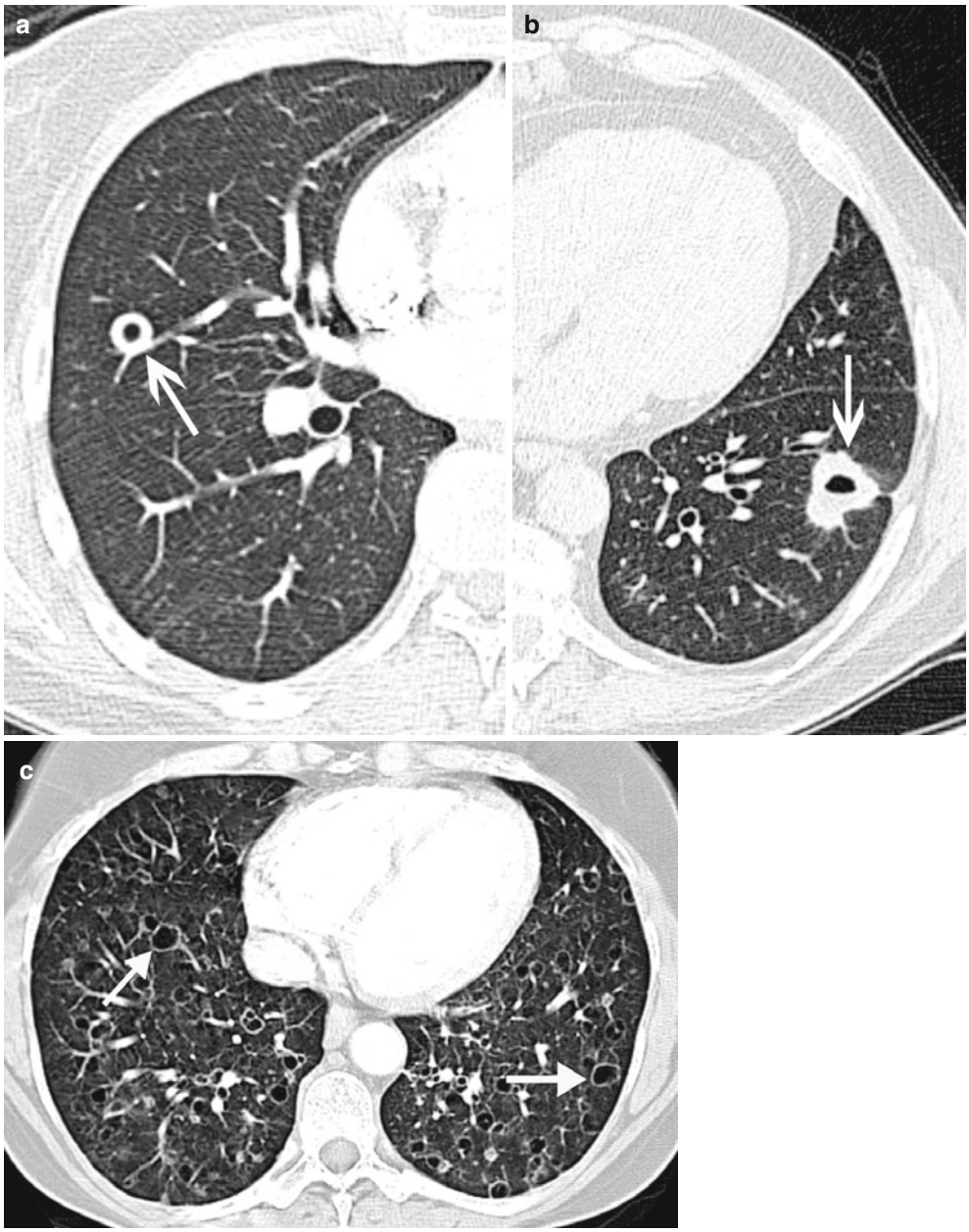

Fig. 1.20 Chest CT scans with lung window settings showing cavitary metastases in the lung. (**a**) A well-circumscribed round nodule with a central lucency (*arrow*) in a 38-year-old woman with metastatic rectal adenocarcinoma with mucinous features. (**b**) A somewhat irregular nodule with a central lucency (*arrow*) corresponding to pulmonary metastasis in a 62-year-old man with keratinizing squamous cell carcinoma of the tongue. (**c**) Bilateral small cyst-like structures (*arrows*) with thin walls in a 58-year-old woman with widely metastatic adenocarcinoma of the lung

Primary Malignant Pleural Tumors

Mesothelioma

Imaging plays an integral part in the diagnosis, staging, and treatment response assessment of mesothelioma. This disease poses challenges in imaging because of its complex three-dimensional configuration. Treatment options for mesothelioma, which range from conservative management to radical surgery, depend on staging, which requires accurate delineation of the tumor using imaging. Typically, mesothelioma manifests as a unilateral pleural mass with moderate to large pleural effusion. The subtypes of mesothelioma do not have distinct imaging features and are only identified histologically. This locally aggressive tumor rarely metastasizes to distant sites, yet most patients present with advanced disease and die within 1 year after presentation [293–300].

Imaging of Mesothelioma

Malignant pleural mesothelioma (MPM) is often detected first on chest radiographs as a unilateral pleural abnormality with moderate to large effusion [301–305]. In 45–60 % of patients, mesothelioma manifests as a smooth, lobular pleural mass that infiltrates the pleural space and fissures [301–303]. As the tumor grows, it typically encases the lung and causes an

Fig. 1.21 Contrast-enhanced chest CT scan with lung window settings showing multiple small nodules with ground-glass halos in a 38-year-old woman 2 years after treatment of an angiosarcoma of the left breast. The largest nodule (*arrow*) in the right lower lobe is bilobed and measures 2.2 cm in length, including the surrounding ground-glass halo (*arrowheads*)

Fig. 1.22 High-resolution chest CT scan with lung window settings showing nodular interlobular septal thickening (*arrows*) in the lungs bilaterally along with centrilobular nodular densities and multiple ground-glass opacities, which are consistent with lymphangitic carcinomatosis, in a 26-year-old man with previously treated primary colon cancer

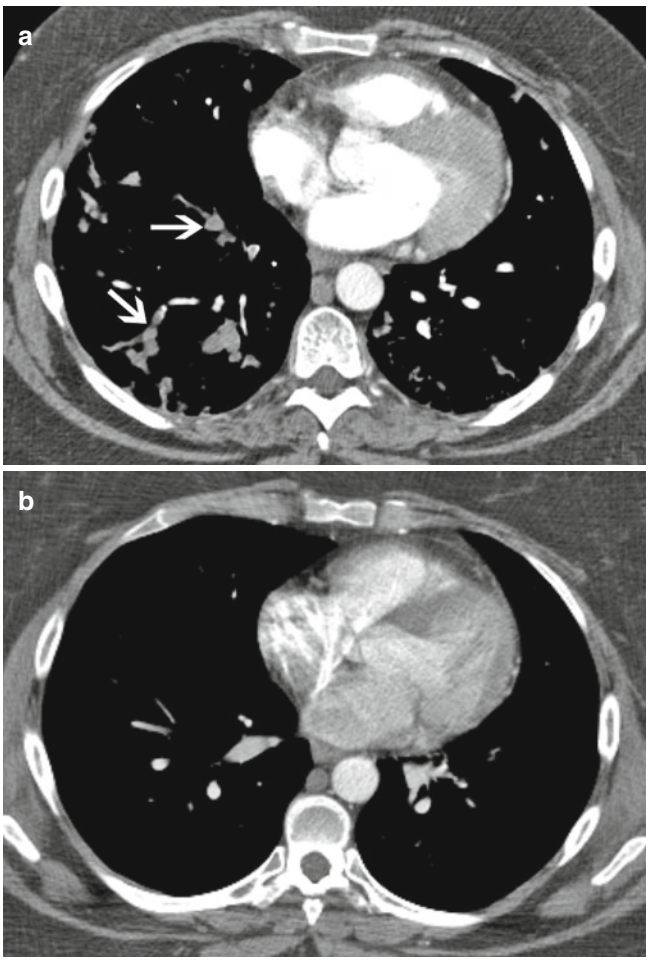

Fig. 1.23 (**a**) Contrast-enhanced chest CT scan with mediastinal window settings demonstrating beading of the pulmonary arteries (*arrows*) secondary to pulmonary arterial tumor emboli in a 41-year-old woman with chondrosarcoma of the right pelvis and sacrum after hemipelvectomy. (**b**) Contrast-enhanced chest CT scan performed 7 months before the scan in (**a**), showing no abnormalities in the pulmonary vessels

ipsilateral shift of the mediastinum with narrowing of intercostal spaces (Fig. 1.25a–d) [305]. Signs of chest wall invasion of MPM on plain chest radiographs are osseous destruction and periosteal reaction of the ribs [302, 305, 306]. Lymph node involvement is rarely assessed using chest radiography because the tumor abuts and obscures the contours of the ipsilateral mediastinum and hilum. Metastasis of MPM to the lungs may produce pulmonary nodules or thickening of the interlobular septa [305, 307, 308] but is uncommon at presentation. Contralateral pleural abnormalities are usually caused by underlying asbestos-related pleural disease, although they can be caused by pleural metastases in rare cases.

Contrast-enhanced multidetector chest CT is the examination of choice for the initial evaluation of MPM and has surpassed MRI as the primary modality for determining the T status of this tumor. To ensure that the entire pleura is evaluated, scanning must include the chest from the thoracic inlet to the level of the L3 vertebra [309]. Occasionally, more caudal imaging may be required if a bulky tumor causes deflection of the hemidiaphragm.

On CT scans, the features of MPM and other metastases to the pleura can overlap. The vast majority of patients with MPM have pleural effusion and nodular pleural thickening, usually with lower zone predominance. Whereas abnormal, nodular-enhancing pleura can be readily demonstrated using CT, this may not be the case early in MPM or following surgical intervention for pleurodesis. Biopsy analysis is required for definitive diagnosis to distinguish between MPM and pleural metastatic disease.

Late in the course of MPM, the tumor grows circumferentially around the lung (Fig. 1.25a–d) [184, 305, 310–314].

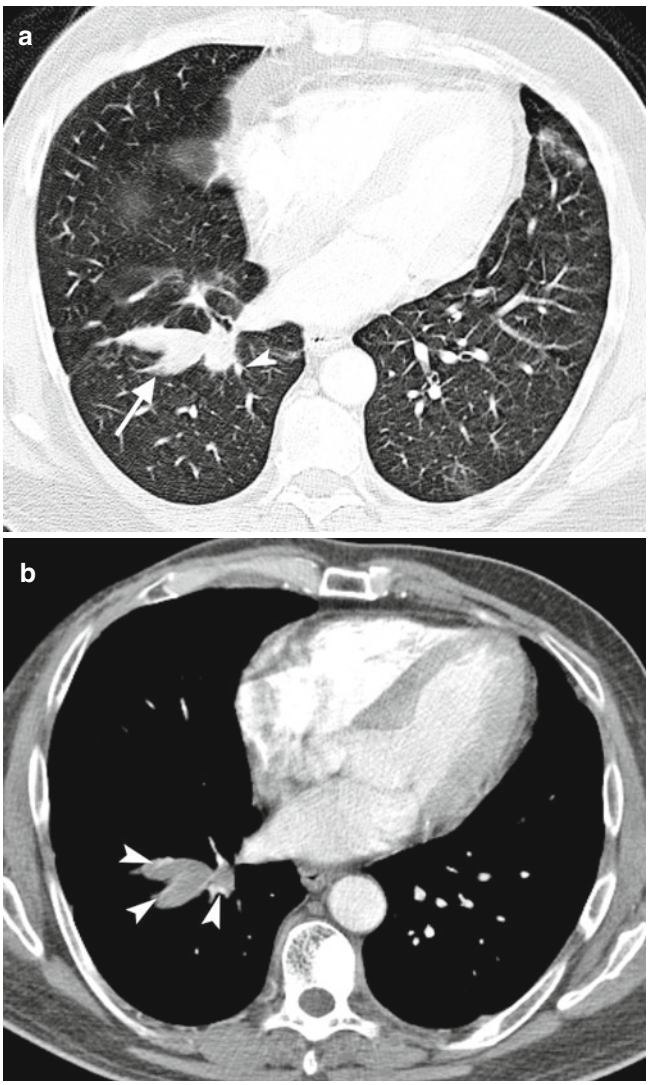

Fig. 1.24 Contrast-enhanced chest CT scan with (**a**) lung and (**b**) mediastinal window settings demonstrating three large tubular opacities appearing to branch in the right lower lobe, which are compatible with metastatic disease in the segmental right lower lobe bronchi, in a 53-year-old man with invasive ductal breast carcinoma that became metastasized. The small high-density linear structures at the periphery of these opacities (*arrowhead*) are the pulmonary vessels running adjacent to the airways

Aggressive tumors can invade local structures. Chest wall invasion obscures and infiltrates the extrapleural fat and intercostal muscles, displaces ribs, and may destroy adjacent bones [310, 313, 315]. Occasionally, CT scans demonstrate focal chest wall involvement at a site of a previous biopsy, surgical scar, or chest tube tract [308]. Direct mediastinal extension of MPM can cause infiltration of fat planes, and concomitant invasion of local mediastinal structures—the great vessels, esophagus, and trachea—may occur; tumor tissue surrounding more than 50 % of a structure strongly suggests invasion [308, 316]. Pericardial invasion of MPM is suggested by nodular pericardial thickening, which may be accompanied by pericardial effusion. Using up-to-date imaging techniques with thin-section images as well as coronal and sagittal reconstructions, radiologists can demonstrate gross diaphragmatic invasion of MPM directly rather than relying solely on indirect signs of tumor diaphragmatic invasion (Fig. 1.26). In assessment of diaphragmatic invasion, a clear fat plane between the inferior diaphragmatic surface and adjacent abdominal organs and a smooth diaphragmatic contour suggest that the tumor does not extend through the diaphragm [316].

CT is limited in the evaluation of mesothelioma. Because of the complex shape of the pleura, differentiating abnormal pleura from adjacent pleural effusion or a collapsed adjacent lung can be difficult. A complicating factor is that many patients with MPM have undergone invasive biopsy or pleurodesis, resulting in inflammatory and/or fibrotic changes that can mimic malignancy by the time of the staging CT scan.

MRI is usually reserved for patients with MPM whose disease is potentially resectable and who have equivocal findings on initial chest CT scans regarding chest wall, pericardial, or diaphragmatic invasion. Marked enhancement of MPM on MRI scans using gadolinium-based contrast agents and the multiplanar imaging capabilities of MRI are particularly useful for delineating multifocal chest wall invasion and transdiaphragmatic invasion by this tumor [317]. The signal intensity of MPM typically is equal to or slightly greater than that of the adjacent chest wall muscle on T1-weighted images and moderately greater on T2-weighted images. Administration of a contrast agent produces intense enhancement of the pleural tumor. As on CT scans, loss of normal fat planes, gross extension into mediastinal fat, and tumor tissue surrounding more than 50 % of a mediastinal structure on MRI scans all suggest tumor invasion [316].

MPM exhibits ^{18}FDG avidity on PET scans [318–323], but the poor spatial resolution of PET limits its use as the sole imaging method for MPM. However, use of integrated PET-CT has improved identification of regions of MPM involvement with increased ^{18}FDG uptake and the accuracy of staging in patients with MPM [324]. ^{18}FDG-PET does not overcome the limitations of other imaging methods in the evaluation of microscopic transdiaphragmatic invasion of MPM, though. The major strength of ^{18}FDG-PET in imaging MPM is delineation of metastatic spread that is not detected morphologically, including that in lymph nodes and at distant sites. Moreover, authors have reported that ^{18}FDG-PET can predict survival rates in patients with mesothelioma when the entire pleural disease is assessed according to total glycolytic volume but not when disease foci are assessed according to the maximal standardized uptake value [325].